Original article

Integration of pharmacodynamics, metabolomics and network pharmacology to elucidate the effect of *Prunella vulgaris* seed oil in the treatment of hyperlipidemia

Min Zeng [c,1], Xinyi Qin [a,b,1], Tao Yi [c,1], Zixuan Liu [a], Chengfeng Li [c], Shuna Tan [c], Shuai Zhang [a], Tongxin Xie [a], Jingchen Xie [a,b], Ping Wu [a,b], Zhimin Zhang [a,b,*]

[a] *College of Pharmacy, Hunan University of Chinese Medicine, Changsha 410208, China*
[b] *Key Laboratory for Quality Evaluation of Bulk Herbs of Hunan Province, Hunan University of Chinese Medicine, Changsha 410208, China*
[c] *College of Xiangxing, Hunan University of Chinese Medicine, Changsha 410208, China*

ARTICLE INFO

ABSTRACT

To investigate the lipid-lowering activity of PVSO (a natural oil derived from the mature seeds of *Prunella vulgaris* L.), supercritical CO_2 extraction technology was used to extract, and the components were characterized using GC–MS/MS and LC-MS/MS techniques. The lipid-lowering activity of PVSO was evaluated *in vitro* and *in vivo*. The results indicated that the supercritical CO_2 extraction rate of PVSO was 16.63 %, and the ratio of linolenic acid to linoleic acid was 3:1. In addition, PVSO also contains bioactive components such as phenols, terpenes, flavonoids, and squalene. *In vitro* experiments showed that PVSO has a strong inhibitory effect on porcine pancreatic lipase, cholesterol esterase, and cholesterol micellization in a significant dose-dependent manner. *In vivo* experiments showed that PVSO (500 and 800 mg/kg) intervention markedly attenuated body-weight gain, liver weights, hepatic steatosis, oxidative stress biomarkers, and dyslipidemia induced by HFD ($p < 0.05$). Serum metabolomics studies revealed that 29 endogenous metabolites were significantly altered by HFD and recovered following intervention with PVSO ($p < 0.05$). PVSO suppressed hyperlipidemia mainly by regulating oxidative stress, choline metabolism, glycine, serine and threonine metabolism, and cholesterol metabolism. Combining metabolomics and network pharmacology analysis, 17 intersection targets, 21 GO and 6 KEGG pathways were obtained. Molecular docking showed that ACHE, CPT1A, HMGCR, LYPLA1, and PLD2 were the key targets of PVSO against hyperlipidemia. In summary, PVSO might be a potential active resource to prevent oxidative stress and lipid metabolism disorders in HFD-induced hyperlipidemia.

1. Introduction

Hyperlipidemia is a metabolic disorder that is characterized by abnormally high levels of total cholesterol (TC), triacylglycerol (TG), and low-density lipoprotein cholesterol (LDL-C) or low levels of high-density lipoprotein cholesterol (HDL-C) in serum (Onwe et al., 2015). HFD-induced oxidative stress is a process of oxidative damage caused by the accumulation of reactive oxygen species (ROS) in cells, which is closely related to the occurrence and development of hyperlipidemia (Zhao et al., 2017). Statins are the most widely used first-line lipid-lowering drugs in clinical practice, especially in the treatment of hyperlipidemia (Wierzbicki et al., 2012). Clinical liver injury from

statins is very rare, but the use of statins can be associated with abnormal liver function, striated muscle tissue, rash and pruritus, which are related to the frequency of clinical use and the interaction of combined drugs (Björnsson et al., 2017). Using natural ingredients in natural plants to reduce blood lipids and regulate abnormal lipid metabolism has always been a focus of attention at home and abroad.

Prunella vulgaris L., also known as self-heal, is a traditional herbal medicine belonging to the Labiatae family and distributed around the world, mainly in temperate and tropical mountains, such as Europe, Asia, northwest Africa and North America (Bai et al., 2016). In southern China, it is also the main raw material of Guangdong herbal tea, well known as Wanglaoji-Liang-Cha (Qu et al., 2017). In Europe, this plant is

also commonly consumed as food or tea. *Prunella vulgaris* L. displays significant antioxidant, anti-inflammatory, antitumor, anti-atherosclerosis, and anti-hyperlipidemic activities due to its rich polyphenols, triterpenes and polysaccharides (Pan et al., 2022). The seeds of *Prunella vulgaris* L. contained omega-3 rich oil and a high content of polyphenolic compounds, which showed strong antioxidant and anti-inflammatory activities (Danthine et al., 2022). The antibacterial, anti-inflammatory, and immunoregulatory effects of *Prunella vulgaris* L. oil have also been reported (Deng et al., 2022; Li et al., 2022a). However, there is no literature about the antioxidant and hypolipidemic activities of PVSO.

Therefore, in this study, we investigated the intervention effect and potential mechanisms of PVSO on hyperlipidemia. We used a supercritical CO$_2$ extraction device to extract PVSO from *P. vulgaris* seeds and characterize the components of PVSO through GC–MS/MS and LC-MS/MS analysis. Then, the lipid-lowering activity of PVSO *in vitro*, such as on the inhibition effect of pancreatic lipase, cholesterol esterase, and micelle cholesterol solubility, was evaluated. Furthermore, we investigated the protective effect of PVSO on HFD-induced oxidative stress and lipid metabolism disorder in mice. Briefly, serum and liver biochemical analysis, histopathological analysis, and metabolic analysis were performed. Additionally, a combination of serum metabolism and network pharmacology based on PVSO components, and molecular docking analysis were carried out to explore and validate the active components and potential targets of PVSO in the treatment of hyperlipidemia. The results of the present study might provide a nutritional strategy for preventing hyperlipidemia and provide the theoretical basis for the development and application of PVSO as a new active ingredient resource, such as the potential to be developed into functional oils with high utilization value. In addition, this study has far-reaching significance to further increase the comprehensive application of *Prunella vulgaris* L. resources and improve the added value of the *Prunella vulgaris* L. industry.

2. Materials and methods

2.1. Plant material and preparation of PVSO

Prunella vulgaris L. was purchased from Hunan Yafei Traditional Chinese Medicine Slices Co., Ltd. (No. 211201). The plant species identification was confirmed by Professor Limei Lin (College of Pharmacy, Hunan University of Chinese Medicine). Supercritical fluid extraction using CO$_2$ was performed using a laboratory-scale supercritical fluid system (Hangzhou Huali Pump Co., Ltd) to produce PVSO. The extraction conditions were carried out with slight modifications according to Lee et al. (2021). The extraction was performed at 40 ℃, 25 MPa of extraction kettle, 50 ℃, 5 MPa of separation kettle, and constant CO$_2$ flow rate of 15 L/h for 2 h. Then the obtained PVSO was weighted and stored at −80 ℃ until further analysis. The extract yield of PVSO from *Prunella vulgaris* seeds was 16.63 %. The extraction yield (% w/w) was calculated using the following equation:

$$Extract\ yield\ (\%) = \frac{PVSO\ mass\ (g)}{Seeds\ mass\ (g)} \qquad (1)$$

2.2. UHPLC-QE-MS and GC-TOF-MS analysis

1) UHPLC-QE-MS.

Metabolite extraction: PVSO (100 mg) was mixed with 500 μL of −40 ℃ precooled extraction solvent (methanol: water = 4:1, including internal standard 1000:10). The solution was then homogenized (JXFSTPRP-24, Shanghai Jingxin Technology Co., Ltd.) for 4 min under 45 Hz, and sonicated for 1 h in ice-water bath (YM-080S, Shenzhen Fangao Microelectronics Co., Ltd.). After holding at 40 ℃ for 1 h, the extract was centrifuged at 12000 rpm (Heraeus Fresco17, Thermo Fisher

Scientific) for 15 min at 4 ℃. Then, 100 μL of supernatant was taken for injection analysis after 0.22 μM microporous membrane filtration.

Instrumental analysis (Zhao et al., 2017)**:** An UHPLC system (Vanquish, Thermo Fisher Scientific) with a Waters UPLC BEH C18 column (1.7 μm, 2.1 × 100 mm) was used to perform HPLC separation. The mobile phase consisted of 0.1 % formic acid in water (A) and 0.1 % formic acid in acetonitrile (B). Gradient elution was set as follows: from 0 to 11 min, 85–25 % A; from 11 to 12 min, 25–2 % A; from 12 to 14 min, 2–2 % A; from 14 to 14.1 min, 2–85 % A; from 14.1 to 16 min, 85–85 % A. The flow rate was 0.5 mL/min, and the sample injection volume was 5 μL. An Orbitrap Exploris 120 mass spectrometer coupled with Xcalibur software (Thermo Fisher Scientific) was employed to obtain the MS and MS/MS data based on the IDA acquisition mode. The ionization parameters were set as follows: sheath gas flow rate-35 Arb; aux gas flow rate-15 Arb; ion transfer tube and vaporizer temperature-350 ℃; collision energy-16/32/48 eV (NCE mode); spray voltage-5.5 kV (positive) or −4 kV (negative).

2) GC-TOF-MS.

Metabolite extraction: 50 ± 1 mg of sample was weighed into a 2 mL tube and spiked with 450 μL of precooled extraction mixture (methanol/chloroform (v:v) = 3:1) with 10 μL of adonitol (0.5 mg/mL stock) and 10 μL of L-2-chlorophenylalanine (1 mg/mL stock) as internal standards. Solutions were vortexed for 30 s and homogenized with a ball mill at 45 Hz for 4 min, followed by ultrasonication in ice water for 5 min. After centrifugation (12000 rpm, 4 ℃, 15 min), 300 μL of supernatant was transferred to a fresh tube. Sixty microliters of each sample were removed and combined together to prepare the QC (quality control) sample. After evaporation in a vacuum concentrator, 50 μL of methoxyamination hydrochloride (20 mg/mL in pyridine) was added, incubated at 80 ℃ for 30 min, and then derivatized by 70 μL of BSTFA reagent (1 % TMCS, v/v) at 70 ℃ for 1.5 h. After cooling to room temperature, 5 μL of FAMEs (in chloroform) was added to the QC sample. All samples were then analyzed by an Agilent 7890 gas chromatograph coupled with a time-of-flight mass spectrometer (GC-TOF-MS).

Instrumental analysis (Kind et al., 2009)**:** The separations were performed with a DB-5MS capillary column. Helium was used as carrier gas at a flow rate of 1 mL/min, and the injection volume was 1 μL in splitless mode. The initial temperature was kept at 50 ℃ for 1 min. After that the temperature was raised to 310 ℃ at a ramping rate of 10 ℃/min, and then held at 310 ℃ for 8 min. The injection, transfer line, and ion source temperatures were 280, 280 and 250 ℃, respectively. The energy was −70 eV in electron impact mode. The mass spectrometry data were acquired in full-scan mode with a *m/z* range of 50–500 at a rate of 12.5 spectra per second after a solvent delay of 6.25 min. Chroma TOF (V 4.3x, LECO) software was used for raw data analysis, and the LECO-Fiehn Rtx5 database was used for metabolite identification by matching the mass spectrum and retention index.

2.3. Pancreatic lipase inhibition assay

Triglycerides are decomposed into glycerol and fatty acids by pancreatic lipase, so they can be titrated with sodium hydroxide (phenolphthalein as an indicator) to calculate the generation of fatty acids and reflect the activity of pancreatic lipase. The pancreatic lipase inhibitory activity of PVSO was determined according to the method described by Wang et al. (2014) with some modifications. Briefly, 1 mL of homogenized olive oil (substrate) and various volumes of PVSO (0, 5, 10, 15, 20, and 25 μL) were dissolved in 5 mL of 0.025 mol/L sodium phosphate buffer (pH 7.04, containing 0.1 M NaCl) and maintained at 40 ℃ for 5 min. 1 mL of pancreatic lipase (30,000 U/g, purchased from Shanghai Ruiyong Biotechnology Co., Ltd) solution (240 U/mL) was added to this reaction mixture, and then incubated at 40 ℃ for 5 min. After that, 15 mL of 75 % ethanol was immediately added to terminate

the enzyme reaction. With phenolphthalein as the indicator and the reaction mixture without PVSO as the blank control, the released fatty acid was titrated with 0.025 mol/L sodium hydroxide to obtain the molar mass. The amount of the enzyme that released 1 mmol free fatty acid per minute under standard measurement conditions was defined as a "lipase unit". The experiment was conducted in triplicate, with the data presented as the means ± SEMs. The inhibitory rate of a certain PVSO on pancreatic lipase activity was expressed as follows:

$$Inhibition\ (\%) = \frac{A-B}{A} \times 100\% \qquad (2)$$

where *A* is the molar mass of free fatty acid released from pancreatic lipase in the blank control. *B* is the molar mass of free fatty acid released from pancreatic lipase with PVSO.

2.4. Cholesterol esterase inhibition assay

The cholesterol esterase inhibition activity of PVSO was determined spectrophotometrically based on the method of Long et al. (2022). Cholesterol esterase (48 U/mg, purchased from Yuanye Biotechnology Co., Ltd., Shanghai, China) was predissolved in high-purity water (20 µg/mL), and 100 µL of substrate PNPB (purchased from Shanghai Ruiyong Biotechnology Co., Ltd) was predissolved in 2800 µL of acetonitrile. NaCl (0.2925 g) and sodium taurocholate (0.1387 g) were dissolved in 50 mL (0.1 mol/L, pH 7.4) of sodium phosphate buffer solution. Then, 50 µL porcine cholesterol esterase (0.96 U/mL) was mixed into 1 mL of the above solution, and then PVSO at different volumes (0, 5, 10, 15, 20, 25 µL) was added and incubated at room temperature for 5 min. An ultraviolet visible spectrophotometer was used to measure the absorbance at 405 nm after coloring with 10 µL of PNPB. The experiment was performed in triplicate, and data are presented as the means ± SEMs. The percentage inhibition was calculated as

$$Inhibition\ (\%) = \frac{A-B-(C-D)}{A-B} \times 100\% \qquad (3)$$

where *A* and *B* are the absorbance of the blank control with or without the enzyme, respectively. *C* and *D* are the absorbance of PVSO with or without the enzyme, respectively.

2.5. Fluorescence measurements

The effects of PVSO on the fluorescence spectra of pancreatic lipase and cholesterol esterase was determined according to the method of Martinez-Gonzalez et al. (2017), with some modifications. Briefly, 2 mL of the pancreatic lipase or 1.5 mL of the cholesterol esterase solution (final concentration is 0.2 mg/mL) and different volumes (0, 5,10, 15, 20 µL) of PVSO were mixed for 1 min and incubated at 37 °C for 1 h. Then the mixture was centrifuged at 5000 rpm for 15 min. A volume of 1 mL of supernatant was diluted to 3 mL with the phosphate buffer, and a Shimadzu F-6000 fluorescence spectrometer (Shimadzu, Japan) was used to measure the effects of different volumes of PVSO on the fluorescence spectrum of pancreatic lipase or cholesterol esterase. The fluorescence spectrum parameters were as follows: excitation wavelength-280 nm, emission wavelength-300 to 420 nm, slit width of excitation band and emission light-5 nm, data interval-1 nm, and scanning speed-6000 nm/min. Fluorescence quenching was determined using the Stern-Volmer equation (Gan et al., 2013):

$$\frac{F_0}{F} = 1 + K_{sv}[Q] \qquad (4)$$

where F_0 is the fluorescence intensity without PVSO and *F* is the fluorescence intensity after the addition of PVSO. K_{sv} is the Stern-Volmer quenching constant. [Q] is the concentration of PVSO (mg/mL) (Zhang et al., 2020).

2.6. Determination of cholesterol micellization solubility

Cholesterol micelles were prepared according to the method described by Zhu et al. (2022a). Cholesterol (7.70 mg, Sigma) and oleic acid (14.10 mg, Shanghai Macklin Biochemical Technology Co., Ltd) were dissolved in 2 mL methanol and dried with a nitrogen blowing apparatus. Then, 53.77 mg sodium taurocholate (purchased from Shanghai Ruiyong Biotechnology Co., Ltd) and 10 mL sodium phosphate buffer solution (pH 7.4) were added. After 30 min of ultrasound (400 W, 20 kHz) treatment, the micelles were incubated at 37 °C for 24 h.

Then, various amounts of PVSO (0, 2, 4, 6, 8, 10 µL) were added into the 1 mL micellar solution. The micellar solution without PVSO was used as a substrate blank to calculate the recovery. After shaking and mixing, the mixtures were placed at 37 °C for 2 h and then centrifuged at 15000 rpm for 30 min. The cholesterol content in the supernatant was determined by a total cholesterol kit (Nanjing Jiancheng Bioengineering Institute, Jiangsu, China) (Zhang et al., 2012). The inhibition of micelle cholesterol solubility was calculated using the following equation:

$$Inhibition\ (\%) = \frac{A-B}{A} \times 100\% \qquad (5)$$

where *A* is the cholesterol concentration of blank micelles without PVSO, and *B* is the cholesterol concentration of micelles with the addition of PVSO.

2.7. Transmission electron microscopy (TEM)

The study was carried out according to the method described by Vermeer et al. (2008), with some modifications. Complex particles are formed from PVSO and micellar. To observe all the particles formed, micelles were generated using the standard procedure without centrifugation. To prevent micellar particles from adhering to obtain high-resolution imaging, the noncentrifugal mixed micellar suspension was diluted 10 times, and then 10 µL of suspension was applied to 200 mesh porous carbon copper mesh. To obtain a thin liquid membrane, the liquid membrane was dried after removing excess liquid with filter paper, and TEM (HT7800, HITACHI) imaging was observed.

2.8. Animals

Forty-eight male C57BL/6J mice (SPF, 20 ± 2 g) were purchased from Hunan Slack Jingda Experimental Animal Co., Ltd. [Changsha, China, Certificate number: SYXK (Xiang) 2019–0004].

After 1 week of accommodation, the mice were randomly divided into six groups: (1) normal control (CON) group and (2) PVSO control (PVSO-C) group, were fed with a standard normal chow diet (10 kcal% fat, 20 kcal% carbohydrate and 20 kcal% protein); (3) model control (HFD) group, (4) low-dose PVSO (PVSO-L) group, (5) middle-dose PVSO (PVSO-M) group, and (6) high-dose PVSO (PVSO-H) group, were fed with a high fat diet (20 kcal% fat, 44 kcal% carbohydrate and 22 kcal% protein). Meanwhile, mice in the (4–6) group were supplemented with 200, 500, and 800 mg/kg body weight PVSO solution (dissolved in 0.5 % CMC-Na) by gavage once a day; mice in the (1 and 3) group were supplemented with 0.5 % CMC-Na solution by gavage once a day; and mice in the (2) group were supplemented with 800 mg/kg body weight PVSO solution (dissolved in 0.5 % CMC-Na) by gavage once a day. An overview of the experimental design for all groups is shown in Fig. 3A.

The experiment lasted for 10 weeks. At the end of the experimental period, the mice were fasted overnight and anesthetized with pentobarbital sodium. Then, blood samples were collected and centrifuged to obtain serum. Parts of fresh liver tissues were also collected and immediately fixed in 4 % paraformaldehyde for pathological section observation, and the rest were stored at −80 °C for further assays. The control diet (XT310) and the high-fat diet (XT304) were purchased from Jiangsu Xietong Pharmaceutical Bioengineering Co., Ltd. (Nanjing,

China). All the diets were stored at -20 ℃ throughout this study until needed. All animal experiments were approved by the Ethics Animal Care Committee of Hunan University of Chinese Medicine.

2.9. Biochemical analysis

Total cholesterol (TC), total triglyceride (TG), low-density lipoprotein cholesterol (LDL-C), and high-density lipoprotein cholesterol (HDL-C) were measured with commercial kits (Nanjing Jiancheng Bioengineering Institute, Nanjing, China).

According to the manufacturers' instructions, frozen liver tissues were accurately weighed and homogenized with anhydrous ethanol or saline (1:9 (w/v)). Afterward, the liver homogenate was centrifuged (10000 rpm, 4 ℃) for 10 min, and the supernatant was taken for the experiment. The protein concentration in the liver was quantified by the Bicinchoninic Acid (BCA) Protein Colorimetric Assay Kit (Elabscience, Wuhan, China). Then, lipid-related indicators (TC and TG) and oxidative stress parameters in the liver, such as superoxide dismutase (SOD), malondialdehyde (MDA) and glutathione peroxidase (GSH-Px), were analyzed by assay kits (Nanjing Jiancheng Bioengineering Institute, Nanjing, China). Oxidative stress parameters were normalized to the respective protein concentrations.

2.10. Histopathological examination

According to a previous study (Ta et al., 2023), fresh liver tissues fixed in 4 % paraformaldehyde were embedded in paraffin and sectioned, followed by staining with hematoxylin and eosin (H&E) for histopathologic analysis. Liver slides were observed under a microscope (Nikon ECLPSE-Ci).

2.11. Untargeted metabolomics

Referring to the method of Zhou et al. (2019), untargeted metabolomics techniques were used to study the changes in serum metabolites. Briefly, serum samples were mixed with cold methanol/acetonitrile (1:1, v/v) to remove the protein and centrifuged at 14,000 g for 20 min at 4 ℃. The vacuum-dried supernatants were redissolved in 100 μL acetonitrile/water (1:1, v/v) solvent and centrifuged (14000 g, 4 ℃) for 15 min, and then the supernatant was injected.

Ultrahigh-performance liquid chromatography (Vanquish UHPLC, Thermo) coupled to a Q Exactive mass spectrometer (Orbitrap MS, Thermo) was performed for analysis. Briefly, a 2.1 mm × 100 mm ACQUITY UPLC BEH Amide 1.7 μm column (Waters, Ireland) was used for hydrophilic interaction liquid chromatography (HILIC) separation. After sum normalization, the processed data were analyzed by the R package (ropls). The distributions of all samples were observed, and a general overview of changes in metabolic patterns was obtained through principal component analysis (PCA). Variables related to the separation were identified, and the variable influence on projection (VIP) was calculated through orthogonal partial least squares-discriminate analysis (OPLS-DA). Metabolites with VIP > 1 and p values < 0.05 (Student's t test) were defined as significantly different metabolites (DEMs).

2.12. RNA isolation and real-time quantitative PCR analysis in liver

Total RNA was extracted from frozen liver tissue using TRIzol

reagent (Sangon Biotech, Shanghai, China), and reverse transcription was performed according to the manufacturer's instructions for the RevertAid RT Reverse Transcription Kit (Thermo Scientific, USA). The mRNA levels were quantified using a real-time PCR system (QuantStudio^{TM}1 Plus System, ABI/Thermo, USA) with 2X SG Fast qPCR Master Mix (High Rox) (Sangon Biotech, Shanghai, China) as previously described (Liu et al., 2021). The PCR conditions were as follows: 95 ℃ for 3 min for initiation, followed by 45 cycles of 15 s at 95 ℃ and 30 s at 60 ℃. The primers of the target genes are shown in Table 1. Relative expression of the target gene was normalized to the expression of β-actin by the $2^{-\Delta\Delta Ct}$ method.

2.13. Integrative analysis of the network pharmacology and metabolomics

Integrated metabolomics and network pharmacology analysis was performed as described previously (Zhang et al., 2022b).

The potential targets related to PVSO: 262 ingredients of PVSO (Similarity > 80 %) identified by LC-MS/MS and GC–MS/MS were searched through SwissADME (https://www.swissadme.ch/index.php) with the SMILES obtained from PubChem (https://pubchem.ncbi.nlm.nih.gov) to select the ingredients with high GI absorption and at least two terms of druglikeness were YES. Since then, 200 ingredients meeting the above criteria have been considered to be potential active ingredients. Then, the potential active ingredients were imported into Swiss Target Prediction (https://www.swisstargetprediction.ch) to identified the potential target proteins under the condition of "Probability*>0.1″ and deleting duplicate targets.

The potential targets related to hyperlipidemia: The targets related to h-yperlipidemia were obtained from Online Mendelian Inheritance in Man databas-e (OMIM, https://www.ncbi.nlm.nih.gov/omim) and GeneCards (https://www.genecards.org/). Finally, the common targets shared by the two databases were retain-ed, while the other targets were removed.

The potential targets related to DEMs: Based on metabolomics, the obtained differential metabolites between HFD and PVSO groups were input into HMDB database to obtain the SMILE format of substances and input into Swiss Target Prediction database to obtain metabolite targets.

Construction of regulation network diagram: Venn diagram of potential targets from PVSO active ingredients, serum metabolomics, and hyperlipidemia disease was drawn to find out intersection targets (overlapped genes) by using an online network drawing tool (https://bioinformatics.psb.ugent.be/webtools/Venn/). The protein–protein interaction (PPI) network diagram was obtained by importing the intersection targets into String (https://string-db.org/Version 10.5) website and visualizing with Cytoscape 3.8.2 software. The nodes in the network are ranked according to the Degree by using the CytoHubba plug-in of Cytoscape 3.8.2, and the top 10 targets were selected as potential core targets. Furthermore, the intersection targets were imported into the Metpascape website (http//metascape.org/) for GO function and KEGG pathway enrichment analysis. The pathway with $p < 0.05$ was screened. Potential active ingredients corresponding to 17 core targets from the PVSO were selected as active ingredients, and DEMs corresponding to 17 core targets were selected as target DEMs. The intersection targets, active ingredients, target DEMs, and KEGG pathway were imported into Cytascape 3.8.2 software to build an "Active ingredients-Targets-KEGG pathway-Hyperlipidemia" network. The top 5 ingredients were selected as the key ingredients based on the degree

Table 1
Primers used for real-time PCR.

Gene	Forward Primer (Sequence 5'-3')	Reverse Primer (Sequence 5'-3')	Target size (bp)
SOD1	CAATGTGACTGCTGGAAAGGA	GCCAATGATGGAATGCTCTC	88
GPX1	AGGAGAATGGCAAGAATGAAGA	AGGAAGGTAAAGAGCGGGTG	136
β-actin	GTGCTATGTTGCTCTAGACTTCG	ATGCCACAGGATTCCATACC	174

SOD1: superoxide dismutase 1; GPX1: glutathione peroxidase 1.

value and relative contents, and 5 key targets were obtained at the same time. Then, molecular docking analysis was conducted between these key ingredients and targets.

2.14. Molecular docking

The crystal structures were collected from the RCSB PDB (htt ps://www.rcsb.org/). The pre-processed target receptors and ligands were processed in the way of ultra-precise molecular docking based on the grid algorithm with all functional residues retained in the grid. The structure of the ligands remained flexible to produce different conformations and the calculations were performed in OPLS force fields. Schrodinger Maestro 11.9 (https://www.schrodinger.com/) was used for all computational calculations.

(A)

(B)

(C)

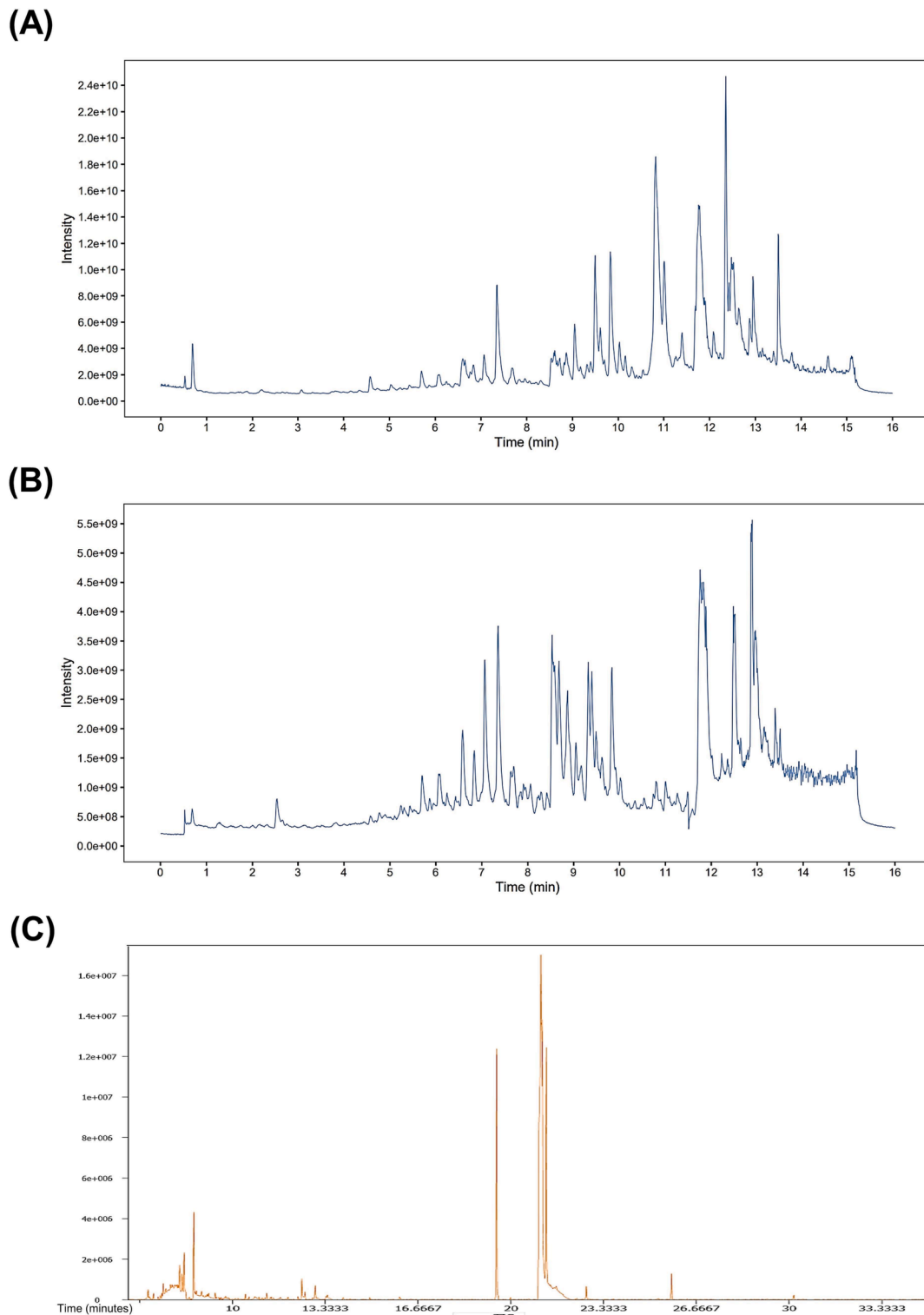**Fig. 1.** Total ion chromatogram (TIC) of PVSO acquired by LS-MS and GS-MS. The relative standard deviation (RSD) ≤ 30 % was used to select 21,514 metabolites, ion numbers in the positive (ESI +) mode (B) and 20,675 in the negative (ESI-) mode (A). Total ion chromatogram (TIC) of PVSO acquired by GS-MS (C).

2.15. Statistical analysis

Origin 8.5 software was used for linear fitting, and GraphPad Prism 8.0 was used for statistical analysis. Two-way analysis of variance (ANOVA) followed by multiple comparisons test and one-way analysis of variance (ANOVA) followed by Dunnett's multiple comparisons test or Tukey's multiple comparison test were used to compare multiple groups (Gosis et al., 2022). Values are presented as the mean ± standard error of the mean (SEM), and $p < 0.05$ was considered statistically significant.

3. Results

3.1. Compounds in PVSO

3.1.1. UPLC-MS/MS

PVSO detected 21,514 peaks in the positive (ESI +) ion mode (Fig. 1A), of which 272 compounds were identified (Table S1, Supplementary Materials). The peak area normalization method was used to calculate the relative percentage content of each component. PVSO in the positive ion mode mainly involves eight categories (Table 2), including terpenoids, fatty acids, phenylpropanoids, alkaloids, phenols, quinones, aromaticity, and flavonoids. The main components of PVSO were (10E,12E)-9-hydroxyoctadeca-10,12-dienoic acid (1.97 %), alpha-linolenic acid (0.23 %), 11,17,21-trihydroxypregn-4-ene-3,20-dione (0.22 %), lucidenic acid M (0.19 %), glyceryl linolenate (0.17 %), dihydroactinidiolide (0.13 %), grandisin (0.10 %), bryonolic acid (0.10 %), loliolide (0.09 %), betulin (0.09 %), etc.

A total of 20,675 peaks were detected according to the negative (ESI-) MS/MS spectrum (Fig. 1B), of which 79 compounds were identified (Table S2, Supplementary Materials). The peak area normalization method was used to calculate the relative percentage content of each component. PVSO in the negative ion mode mainly involves seven categories (Table 3), including fatty acids, terpenoids, phenylpropanoids, phenols, flavonoids, aromaticity, and alkaloids. The main components of PVSO were 9-hydroxy-10,12,15-octadecatrienoic acid (1.66 %), 9E,11E-linoleic acid (0.36 %), azelaic acid (0.27 %), 13-HODE (0.26 %), honokiol (0.14 %), 12,13-EODE (0.14 %), cholic acid (0.11 %), trans- vaccenic acid (0.10 %), etc.

Table 2
Positive ion mode.

Class	Number	Peak area	Relative content (Accounting for all peaks)	Relative content (Accounting for identified peaks)
Terpenoids	100	3.7142×10^9	1.38 %	25.39 %
Fatty acids	4	6.5421×10^8	0.24 %	4.47 %
Phenylpropanoids	16	4.8385×10^8	0.18 %	3.31 %
Alkaloids	15	4.4178×10^8	0.16 %	3.02 %
Phenols	11	2.9401×10^8	0.11 %	2.01 %
Quinones	3	1.6863×10^8	0.06 %	1.15 %
Aromaticity	4	9.2493×10^7	0.03 %	0.63 %
Flavonoids	13	8.7691×10^7	0.03 %	0.60 %
Others	106	4.6343×10^8	3.24 %	59.14 %
Identified peaks	272	1.4627×10^{10}	5.45 %	
Unknown peaks	21,242	2.5394×10^{11}	94.55 %	
All peaks	21,514	2.6857×10^{11}		

Table 3
Negative ion mode.

Class	Number	Peak area	Relative content (Accounting for all peaks)	Relative content (Accounting for identified peaks)
Fatty acids	11	7.5158×10^8	0.69 %	16.06 %
Terpenoids	21	4.8510×10^8	0.44 %	10.36 %
Phenylpropanoids	11	4.1490×10^8	0.38 %	8.86 %
Phenols	8	1.8767×10^8	0.17 %	4.01 %
Flavonoids	7	4.7724×10^7	0.04 %	1.02 %
Aromaticity	4	4.2863×10^7	0.04 %	0.92 %
Alkaloids	2	1.0804×10^7	0.01 %	0.23 %
Others	15	2.7406×10^9	2.51 %	58.54 %
Identified peaks	79	4.6812×10^9	4.29 %	
Unknown peaks	20,596	1.0455×10^{11}	95.71 %	
All peaks	20,675	1.0923×10^{11}		

3.1.2. GC–MS/MS

In the GC–MS analysis, a total of 659 peaks (Fig. 1C) were detected in PVSO, and 249 compounds were identified by searching the LECO Feehn Rtx5 database (Table S3, Supplementary Materials). The relative percentage content of each component was calculated by the peak area normalization method. Ten categories were mainly involved (Table 4), including fatty acids, carboxylic acids and derivatives, terpenoids, amino acids and derivatives, carbohydrates, sterol lipids, phenols, flavonoids, alkaloids, and phenylpropanoids. The main components of PVSO were stearic acid (20.22 %), palmitic acid (18.69 %), 3-

Table 4
The classification of compounds by GC–MS analysis.

Class	Number	Peak area	Relative content (Accounting for all peaks)	Relative content (Accounting for identified peaks)
Fatty acids	17	6.8830×10^7	43.15 %	52.09 %
Carboxylic acids and derivatives	19	2.4383×10^7	15.29 %	18.45 %
Terpenoids	3	8.5304×10^6	5.35 %	6.46 %
Amino acids and derivatives	29	4.2511×10^6	2.66 %	3.22 %
Carbohydrates	6	2.8140×10^6	1.76 %	2.13 %
Sterol lipids	4	8.6223×10^5	0.54 %	0.65 %
Phenols	5	4.4158×10^5	0.28 %	0.33 %
Flavonoids	6	1.2183×10^5	0.08 %	0.09 %
Alkaloids	4	7.7109×10^4	0.05 %	0.06 %
Phenylpropanoids	2	6.0055×10^4	0.04 %	0.05 %
Others	154	2.1767×10^7	13.65 %	16.47 %
Identified peaks	249	1.3214×10^8	82.83 %	
Unknown peaks	313	2.7383×10^7	17.17 %	
All peaks	562	1.5952×10^8		

hydroxypropionic acid (8.34 %), squalene (5.32 %), 3-aminoisobutyric acid (2.69 %), linolenic acid (1.72 %), β-alanine (1.50 %), hydroxylamine (1.32 %), 2-hydroxypyridine (1.22 %), glycerol (1.02 %), oleic acid (1.00 %), and linoleic acid (0.53 %). The ratio of linolenic acid to linoleic acid in PVSO was approximately 3:1.

3.2. Effect of PVSO on the activity of pancreatic lipase and cholesterol esterase

The inhibitory effect of PVSO on pancreatic lipase and cholesterol esterase activities is presented in Fig. 2A and B. PVSO inhibited the activities of pancreatic lipase and cholesterol esterase in a dose-dependent manner, with IC50 values of 1.68 and 3.964 mg/mL, respectively. The inhibitory effect of PVSO on pancreatic lipase is stronger than that on cholesterol esterase.

3.3. Fluorescence quenching measurements

The fluorescent amino acid residues contained in proteins are attributed to the endogenous fluorescence of proteins. These amino acid residues (especially Trp residues) contain conjugated double bonds or benzene ring structures, which can absorb and emit fluorescence (Huang et al., 2020). The interaction of chromophores and quenching agents may lead to a decrease in fluorescence quantum yield, and changes in the tertiary structure of the protein may lead to changes in intrinsic fluorescence emission (Su et al., 2016b; Sun et al., 2016). Therefore, in the absence and presence of PVSO, fluorescence spectroscopy can be used to detect the fluorescence characteristics of proteins, reflecting changes in protein fluorophores and determining structural changes in proteins.

As shown in Fig. 2C and D, the relative fluorescence intensity of pancreatic lipase and cholesterol esterase treated with PVSO decreased with increasing PVSO concentration, which indicates that PVSO can quench the endogenous fluorescence of pancreatic lipase and cholesterol esterase. We speculate that this is because PVSO interacts with pancreatic lipase or cholesterol esterase to form a complex that can quench the enzyme, resulting in changes in the tertiary structure of these enzymes. However, PVSO did not affect the maximum wavelength of fluorescence emission, reflecting that PVSO could not cause changes in the microenvironment of Trp residues in pancreatic lipase or cholesterol esterase. According to literature reports, the fluorescence quenching effect of proanthocyanidin and astaxanthin on pancreatic lipase was also not generated by changing the microenvironment of Trp in pancreatic lipase (Du et al., 2018). As shown in Fig. 2E and F, the value of Ksv for pancreatic lipase (0.09 mL/mg) was lower than that for cholesterol esterase (0.10 mL/mg), indicating that PVSO was more effective in quenching the intrinsic fluorescence of cholesterol esterase, with more affinity.

3.4. The inhibitory effect of PVSO on cholesterol micellization solubility

Approximately 50 % of cholesterol in the intestine is absorbed, while the rest is excreted through feces (Jesch et al., 2017). Cholesterol absorption in the small intestine is closely related to the concentration of total and low-density lipoprotein cholesterol in the plasma; thus, the efficiency of cholesterol absorption in the small intestine has attracted great interest (Jesch et al., 2017). Dietary cholesterol must be incorporated into bile salt micelles before absorption. Therefore, inhibiting cholesterol solubility in micelles and subsequently inhibiting its absorption can effectively reduce cholesterol. For example, green tea catechins, especially those with galloyl moieties, can reduce the micellar solubility of cholesterol through their hydrophobic domains (Ogawa et al., 2016). Therefore, interfering with the formation of cholesterol micelles in the intestine may contribute to the prevention of hyperlipidemia.

In the present study, when PVSO at different concentrations was added to the bile salt micelle solution, it was observed that the solution immediately became turbid (Fig. 2G). PVSO reduced the solubility of cholesterol in bile salt micelle solution in a dose-dependent manner. The highest inhibition rate on cholesterol micelle solubility was 48.29 ± 1.08 %, with 6.60 mg/mL of PVSO (Fig. 2H).

3.5. TEM

As shown in Fig. 2I, the particle size of the cholesterol micelle was small, but after adding PVSO, a composite micelle with a larger particle size was formed between cholesterol and PVSO. Based on Fig. 2G and H, we speculate that the inhibition of cholesterol micelle solubility by PVSO may be due to the interaction between PVSO and cholesterol leading to an increase in the particle size of the complex, as well as the formation of a coprecipitated complex of PVSO and cholesterol in the micelle solution (Zhang et al., 2020).

3.6. PVSO decreased body weight and liver index in HFD-treated mice

As shown in Fig. 3B-F, HFD-fed mice showed significantly higher final body weights and liver weights (p < 0.05) but no significant difference in weight gain and liver index compared with mice in the CON group. PVSO supplementation markedly decreased final body weights and weight gain, as well as liver weights, in a dose-dependent manner compared with the HFD group (p < 0.05), but did not alter the liver index. Furthermore, during the whole experiment, no mouse deaths and no significant differences in the final body weights, weight gain, and liver index were found in the PVSO-C group. These results indicated that PVSO could ameliorate body weight and liver weight gain in mice induced by a HFD diet without side effects.

3.7. PVSO decreased lipid accumulation in HFD-treated mice

Parameters relevant to lipid metabolism in both serum and liver were evaluated (Fig. 4A-E). Specifically, serum TC and LDL-C levels increased in mice fed the HFD compared to the CON group, while HDL-C significantly decreased (p < 0.05). However, medium-dose and high-dose PVSO remarkably reversed the changes in TC content in comparison with the HFD group (p < 0.05). Among them, the TC level distinctly decreased by 17.13 % and 13.99 % in the PVSO-M and PVSO-H groups, respectively. Moreover, the contents of TG and LDL-C in the PVSO-M and PVSO-H groups also showed a downward trend. Liver TC and TG levels of mice in the HFD group were higher than those in the CON group, which were significantly decreased with 500 mg/kg PVSO supplementation (p < 0.05; Fig. 4F, G). The 800 mg/kg PVSO intake also significantly reduced the content of TC (p < 0.05) and showed a decrease in the TG content of mice compared with the HFD group (Fig. 4F, G).

Hepatic lipid accumulation was evaluated by H&E staining of liver sections in mice to determine whether PVSO reduced hepatic steatosis induced by a high-fat diet. The results showed that HFD supplementation led to cellular vacuolization, fatty changes, and inflammatory cell infiltration, while PVSO supplementation improved the alteration of liver structure in a dose-dependent manner (Fig. 4H).

3.8. PVSO improved the oxidative stress parameters and relative mRNA expression levels of liver tissues in HFD-fed mice

Enhanced lipid peroxidation levels may be one of the main pathogenic factors of HFD-induced oxidative stress. As a landmark product of oxidative stress, MDA indicates the process of lipid peroxidation in the liver, which accumulates in the body and is toxic to cells (Khafaga et al., 2017; Ahmed et al., 2020). SOD is an important part of the oxidation protection system, which can alleviate oxidative stress by catalyzing the dismutation of superoxide radicals. GSH is also the most important cellular antioxidant. The reduced activity of antioxidant enzymes (especially SOD) will increase the level of lipid peroxidation and serve as
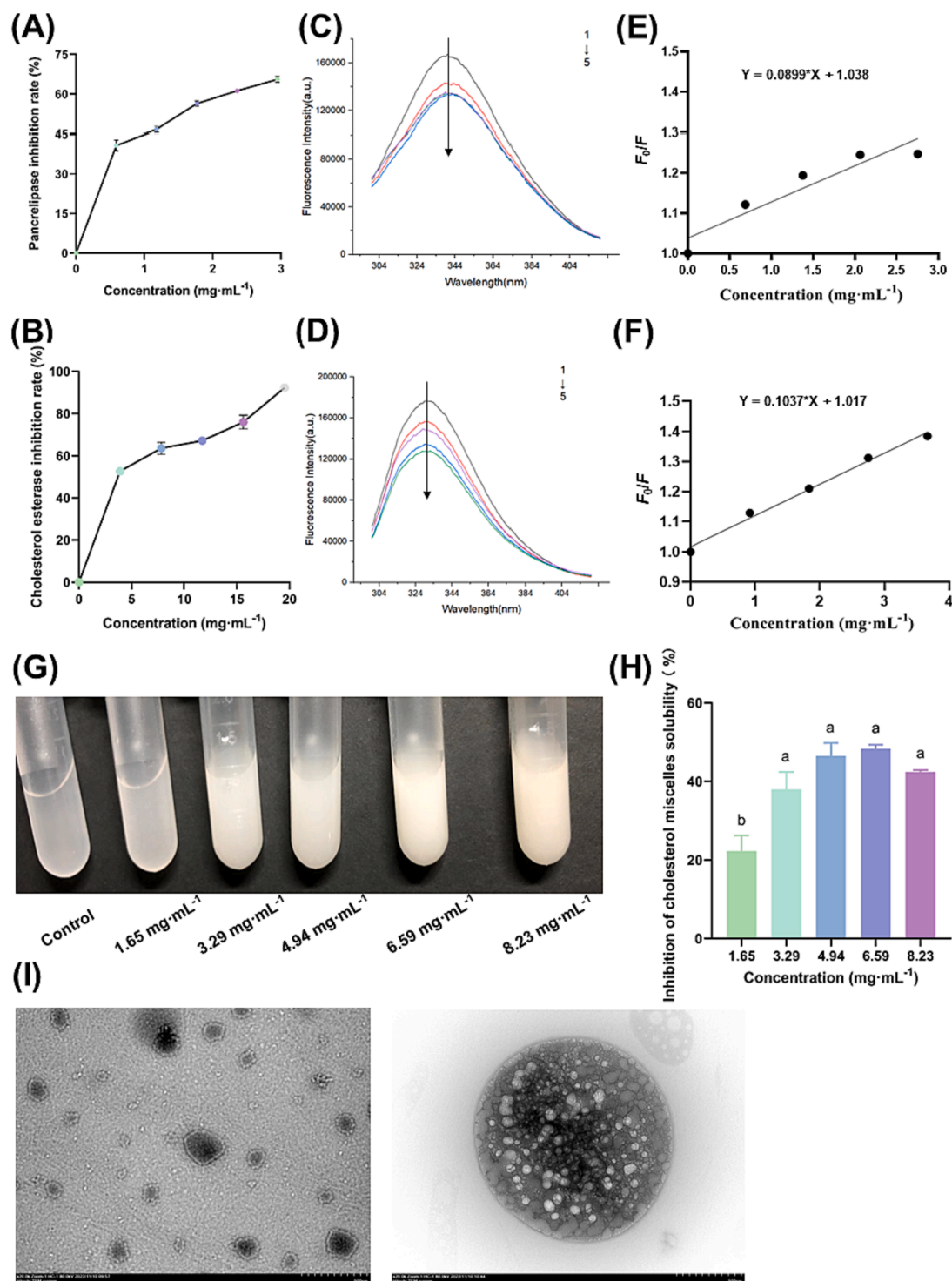
Fig. 2. The lipid-lowering activity of PVSO in a simulated intestinal environment. (A) The inhibition rate of PVSO on pancreatic lipase at different concentrations (0, 0.59, 1.18, 1.77, 2.36, 2.95 mg/mL). (B) Inhibition rate of PVSO on cholesterol esterase at different concentrations (0, 3.91, 7.82, 11.73, 15.64, 19.55 mg/mL). (C) The pancreatic lipase of PVSO treated with different concentrations (0, 0.69, 1.38, 2.06, 2.75 mg/mL) was analyzed by fluorescence spectroscopy. (D) The cholesterol esterase of PVSO treated with different concentrations (0, 0.92, 1.83, 2.75, 3.67 mg/mL) was analyzed by fluorescence spectroscopy. (E) Fluorescence spectra of pancreatic lipase treated with different concentrations of PVSO and Stern-Volmer plot of PVSO fluorescence quenching of pancreatic lipase (λem = 340 nm). (F) Fluorescence spectra of cholesterol esterase treated with different concentrations of PVSO and Stern-Volmer plot of PVSO on fluorescence quenching of cholesterol esterase (λem = 330 nm). (G) PVSO (0, 1.65, 3.29, 4.94, 6.59, and 8.23 mg/mL) was added to a bile salt micellar solution containing cholesterol *in vitro* to form precipitates. When different concentrations of PVSO were added to the bile salt micelle solution, it was observed that the solution immediately became turbid. (H) Effect of PVSO on the solubility of cholesterol micelles. The results are expressed as the mean ± SEM deviation, with different letters indicating significant differences ($p < 0.05$). (I) TEM. The left is blank cholesterol micelle, while the right is cholesterol compound micelle containing 8 mg/mL PVSO.
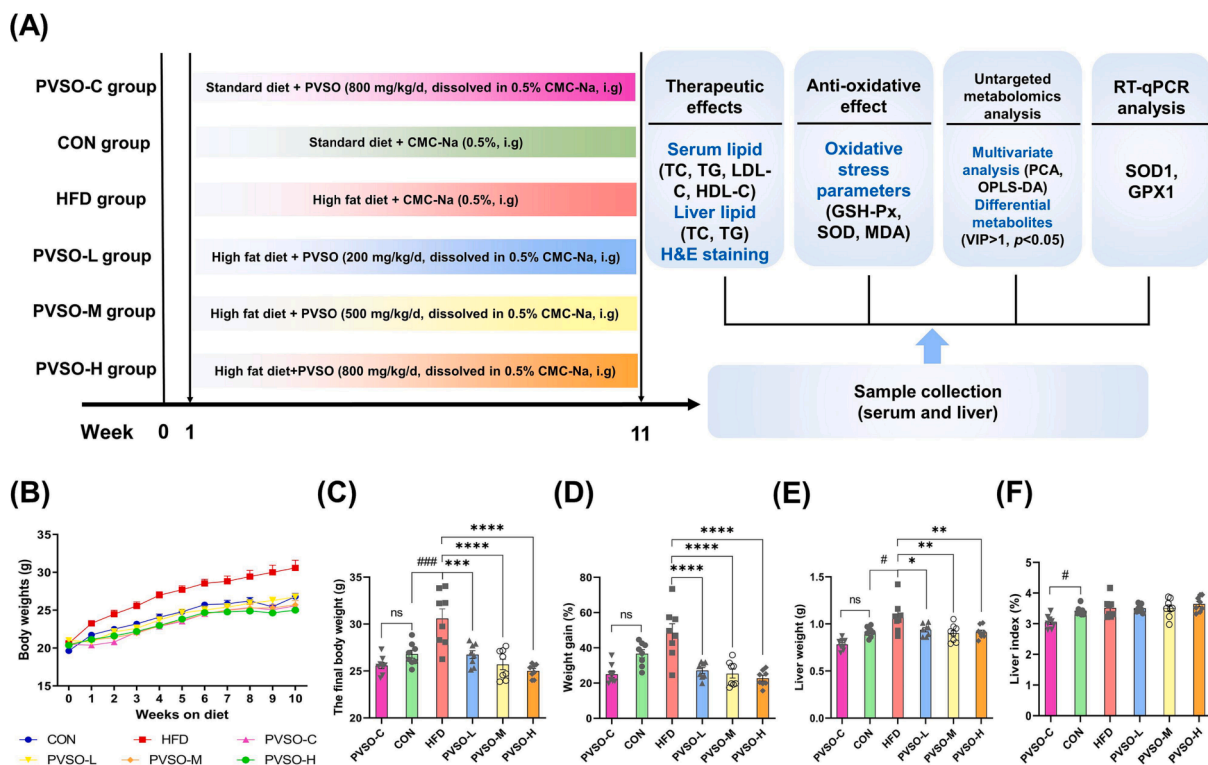
Fig. 3. Effect of PVSO supplementation on body and liver weights in HFD-fed mice. (A) Animal experimental design. (B) Body weight changes, (C) final body weights, (D) weight gain, (E) liver weights, and (F) liver index (liver: body weight). Data are represented as the means ± SEMs (n = 8). The differences were evaluated using two-way analysis of variance (ANOVA) followed by multiple comparisons test (B) or one-way ANOVA with Tukey's multiple comparisons test (C-F) and denoted as follows: $^{\#}p < 0.05$, $^{\#\#}p < 0.01$, and $^{\#\#\#}p < 0.001$, compared with the CON group; $^{*}p < 0.05$, $^{**}p < 0.01$, $^{***}p < 0.001$, compared with the HFD group.
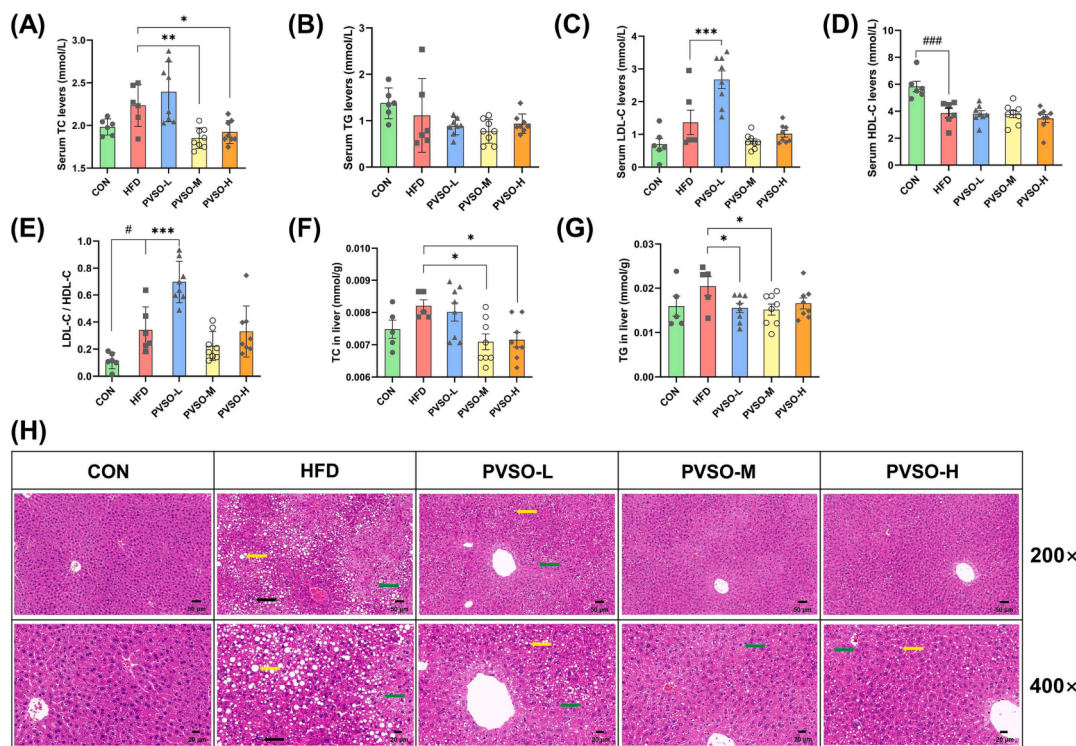

Fig. 4. Effect of PVSO supplementation on the lipid profiles of HFD-fed mice. (A-D) The content of serum TC, TG, HDL-C, and LDL-C. (E) The ratio of LDL-C/HDL-C. (F-G) The content of hepatic TC and TG. (H) Histological assessment of the liver. The liver sections were stained with hematoxylin and eosin, and green, yellow and black arrows indicate hepatocyte cytoplasmic vacuolation, fatty changes, and inflammatory infiltration, respectively. Data are expressed as the means ± SEMs (n = 5–8). The differences were assessed by one-way ANOVA with Dunnett's multiple comparisons test and denoted as follows: $^{\#}p < 0.05$, $^{\#\#}p < 0.01$, and $^{\#\#\#}p < 0.001$, compared with CON; $^{*}p < 0.05$, $^{**}p < 0.01$, $^{***}p < 0.001$, compared with HFD.

an indicator of oxidative stress in different tissues. This study further investigated the effect of PVSO on oxidative stress by measuring liver SOD and GSH-PX activities, as well as MDA levels, in each group of mice. As depicted in Fig. 5A-C, HFD significantly increased the content of MDA and decreased the activity of SOD and GSH-Px in the liver compared with the CON group ($p < 0.05$). After supplementation with PVSO, the level of MDA was decreased by 44.35 %, 50.98 %, and 41.95 % in the PVSO-L, PVSO-M, and PVSO-H groups, respectively. Moreover, PVSO significantly increased the activity of SOD and GSH-Px in the livers of mice ($p < 0.05$). These results indicated that PVSO alleviated oxidative injury induced by a high-fat diet and enhanced the antioxidant capacity of mouse liver tissue.

To further understand the relieving effect of PVSO on oxidative stress in HFD mice, we evaluated the expression of oxidative stress-related genes. HFD significantly reduced the expression of SOD1 and GPX1 genes in the liver compared with the CON group ($p < 0.05$; Fig. 5D, E). In contrast, the relative mRNA levels of GPX1 were slightly recovered in the mouse livers with 500 mg/kg PVSO intake ($p > 0.05$; Fig. 5E).

3.9. Effects of PVSO on the serum metabolic profile

The above results indicated that the middle dose of PVSO exhibited significant therapeutic effects in improving oxidative stress and lipid metabolism disorders. Therefore, the PVSO-M group was selected for subsequent untargeted metabolomics analysis.

The PCA plots showed that the CON group and HFD group could be clearly separated, indicating significant changes in metabolites in mouse serum. In addition, the HFD group and PVSO group can also be clearly separated, indicating that there are also significant differences in metabolites between the two groups (Fig. 6A). To identify the differential metabolites, an OPLS-DA model was used. The OPLS-DA score plot shows a significant separation between the CON and HFD groups, as with the HFD and PVSO groups. To avoid overfitting, we performed OPLS-DA model verification (Permutation test n = 200). The coefficient of determination (R^2) and predictive power (Q^2) of the model were evaluated. These values between the HFD and CON groups were $R^2 = 0.99$ and $Q^2 = 0.707$. Similarly, the values between the PVSO and HFD groups were $R^2 = 0.987$ and $Q^2 = 0.685$ (Fig. 6B, C). These results indicated that the model does not exhibit overfitting and has good stability and predictive ability.

Based on OPLS-DA results, differential metabolites (DEMs) were screened through VIP values (VIP > 1) and p values ($p < 0.05$). As a result, a total of 172 DEMs were screened between the HFD and CON groups, of which 75 and 97 DEMs were identified in POS and NEG ionization, respectively (Table S4, Supplementary Materials). Furthermore, we screened significantly upregulated or downregulated DEMs through fold changes (FC) > 1.2 or < 0.833. There were 52 significantly upregulated DEMs and 112 significantly downregulated DEMs in the HFD group compared to the CON group (Fig. 6D). After intervention with PVSO, 130 metabolites changed significantly, of which 53 and 77 DEMs were identified in POS and NEG ionization, respectively. Twenty-seven metabolites were significantly increased and 85 metabolites were
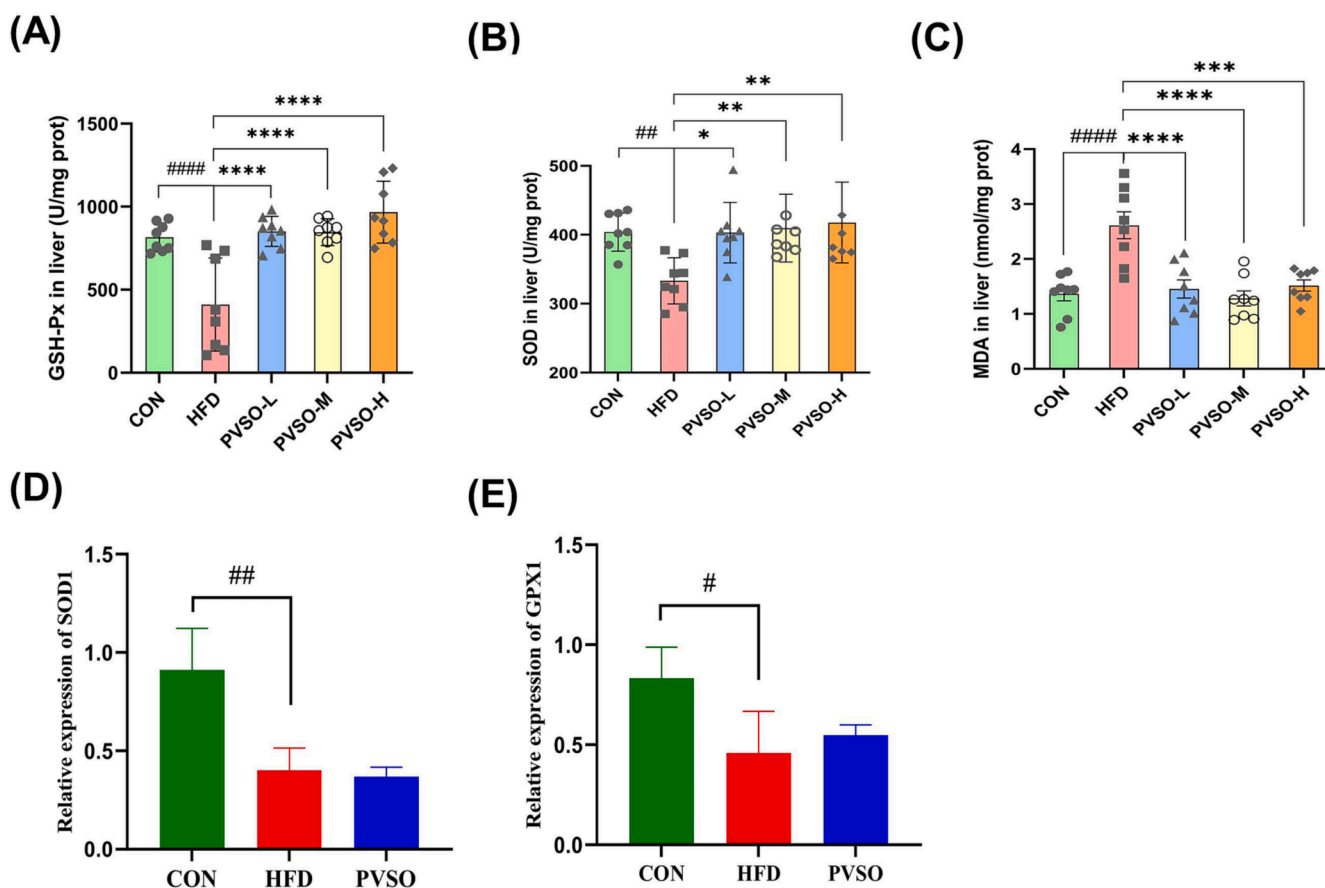

Fig. 5. Effect of PVSO on HFD-induced alterations in oxidative stress marker GSH-Px (A), SOD (B), and MDA (C) levels and relative mRNA expression levels (D-E) of liver samples. Data are expressed as the means ± SEMs (n = 8), and differences were assessed by one-way ANOVA with Dunnett's multiple comparisons test and denoted as follows: $^{\#}p < 0.05$, $^{\#\#}p < 0.01$, and $^{\#\#\#}p < 0.001$, compared with CON; $^{*}p < 0.05$, $^{**}p < 0.01$, $^{***}p < 0.001$, compared with HFD. (D-E) The relative mRNA expression levels related to oxidative stress in the liver. Data are expressed as the means ± SEMs (n = 3), and differences were assessed by one-way ANOVA with Tukey's multiple comparisons test and denoted as follows: $^{\#}p < 0.05$, and $^{\#\#}p < 0.01$, compared with CON. SOD1: superoxide dismutase 1; GPX1: glutathione peroxidase 1.
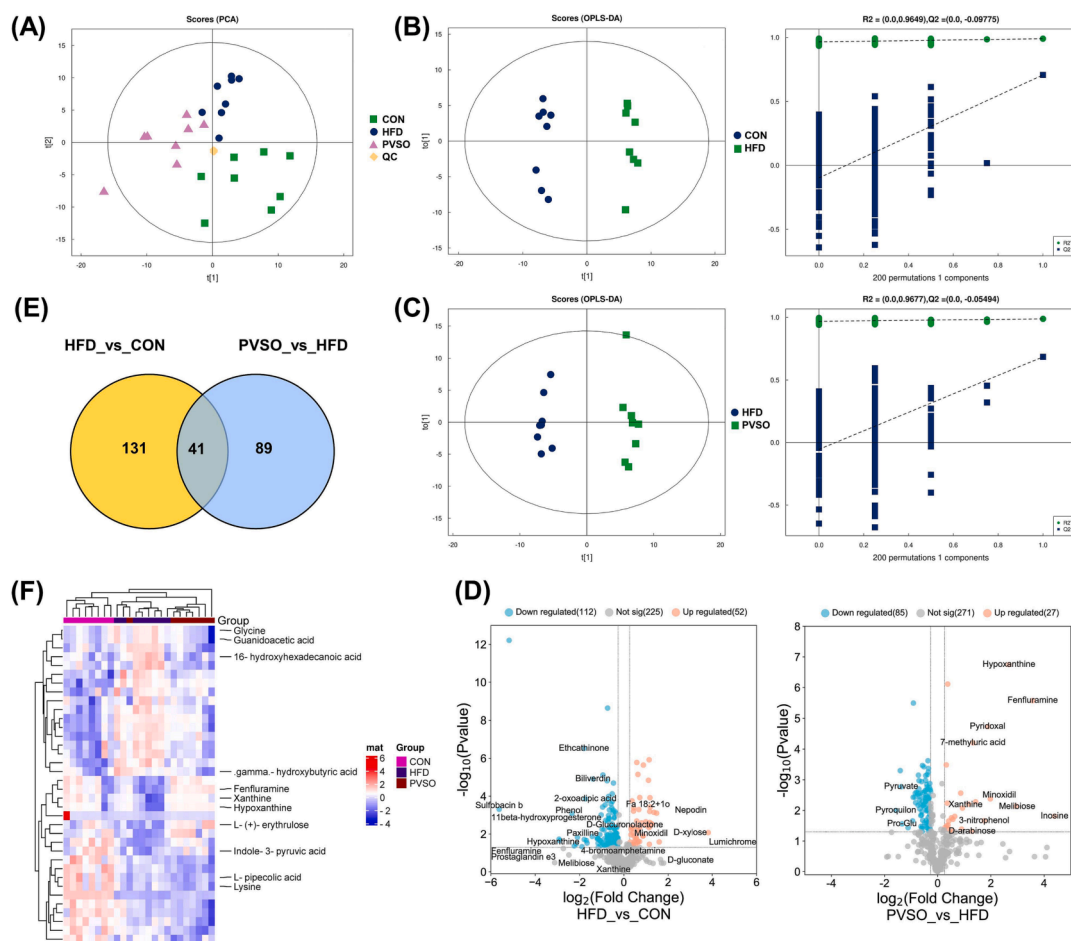
Fig. 6. Multivariate statistical analysis of serum untargeted metabolomics. (A) PCA score plots among the CON, HFD, and PVSO groups. (B-C) Score plots of OPLS-DA. (D) Volcano plots. Fold changes (FC) > 1.2 indicated upregulation, and FC < 0.833 indicated downregulation. (E) Venn plot. (F) Hierarchical clustering heatmap of 36 significantly upregulated or downregulated common DEMs. Each row in the figure represents a differential metabolite, and each column represents a set of samples. Red represents a relatively high expression level of metabolites, while blue represents a relatively low expression level of metabolites. Metabolites with similar expression patterns are clustered in the same cluster on the left.

significantly decreased compared with the HFD group (Fig. 6D; Table S5, Supplementary Materials). Forty-one metabolites were the common DEMs in the two comparison groups (Fig. 6E), of which 36 substances were significantly upregulated or downregulated (Fig. 6F). Among them, 29 substances exhibited opposite trends and were most likely potential biomarkers that have been screened. These biomarkers were divided into the following four categories: lipids and lipid-like molecules (52 %), organoheterocyclic compounds (21 %), organic acids and derivatives (7 %), and others (20 %), including amino acids (e. g., glycine and guanidoacetic acid), fatty acids (e.g., Fa 18:2 + 1o, 16-hydroxyhexadecanoic acid, and gamma-hydroxybutyric acid), indoles and derivatives (indole-3-pyruvic acid), and other endogenous compounds. Compared with the CON group, the levels of 16-hydroxyhexadecanoic acid, 4-(1-piperazinyl)-1h-indole, gamma-hydroxybutyric acid, glycine, guanidoacetic acid, tetrabenazine, etc., were significantly elevated, whereas the levels of indole-3-pyruvic acid, minoxidil, fenfluramine, hypoxanthine, xanthine, 7-methyluric acid, L-(+)-erythrulose, melibiose, etc., were significantly decreased in the serum of mice in the HFD group ($p < 0.05$). Furthermore, compared with the HFD group, PVSO significantly reversed the changes in the above metabolites ($p < 0.05$) (Table 5).

3.10. Metabolic pathway enrichment analysis

Furthermore, we selected the Kyoto Encyclopedia of Genes and Genomes (KEGG, https://www.genome.jp/kegg/pathway.html) database to screen differential metabolic pathways based on the conditions with pathway enrichment impact > 0.05 and $p < 0.05$. The results showed that the differential metabolic pathways between the CON and HFD groups included necroptosis, D-glutamine and D-glutamate metabolism, caffeine metabolism, glycine, serine and threonine metabolism, linoleic acid metabolism, etc. (Fig. 7). The differential metabolic pathways between the HFD and PVSO groups included choline metabolism in cancer, cholesterol metabolism, caffeine metabolism, glycine, serine and threonine metabolism, bile secretion, etc. (Fig. 7). Among them, ABC transporters, butanoate metabolism, caffeine metabolism, central carbon metabolism in cancer, glycine, serine and threonine metabolism, protein digestion and absorption were the common pathways between the CON and HFD groups, as well as between the HFD and PVSO groups. Hence, we focused on discussing these pathways in detail.

3.11. Association analysis

Spearman's correlation analysis showed a correlation between the levels of DEMs in Table 5 and metabolic disorders, including body weights, liver weights, dyslipidemia, and oxidative stress. As shown in Fig. 8A, melibiose, 7-methyluric acid, L-(+)-erythrulose, Pc 38:6, fenfluramine, and hypoxanthine were significantly positively correlated with SOD and GSH-Px activities but negatively correlated with MDA levels ($p < 0.05$). Glycine, guanidinoacetic acid, gamma-hydroxybutyric

Table 5

DEMs in serum after PVSO treatment.

Metabolites	MS Mode	RT [min]	m/z	VIP		FC		Trend		pathway
				H vs. C	P vs. H	H vs. C	P vs. H	H vs. C	P vs. H	
S4:18(p3:16/f1:2)	NEG	28.9938	695.3117	1.1250	1.0296	1.4391	0.7459	↑	↓	
N-palmitoyl-d-sphingosine	NEG	32.2434	536.5046	2.3121	1.1583	2.2051	0.8120	↑	↓	
N-palmitoyl-d-*erythro*-dihydroceramide-1-phosphate	NEG	35.0466	618.4771	9.7923	1.5921	0.0276	1.8222	↓	↑	
Fa 18:2 + 1o	NEG	52.6503	295.2279	7.1278	5.4317	2.5611	0.6440	↑	↓	
16-hydroxyhexadecanoic acid	NEG	54.8142	271.2280	2.7874	3.0886	1.5382	0.6476	↑	↓	1
Indole-3-pyruvic acid	NEG	72.7310	202.0511	2.2979	1.9395	0.6315	1.3073	↓	↑	1,2
Minoxidil	NEG	86.6394	207.9942	1.9982	2.7191	0.2896	3.9390	↓	↑	
Pc 36:2	NEG	124.8160	844.6064	4.4801	3.5010	1.4972	0.7820	↑	↓	
1 h-imidazole, 2-[(1-methylpropyl)dithio]-	POS	142.9490	132.9872	1.2817	1.5325	1.8087	0.3769	↑	↓	
1-palmitoyl-2-docosahexaenoyl-*sn*-glycero-3-phosphocholine	POS	153.2585	806.5691	8.5940	13.9786	0.8892	1.1206	↓	↑	
Pc 38:6	NEG	153.8235	864.5758	3.1548	5.9894	0.8590	1.2966	↓	↑	
Fenfluramine	POS	182.3175	159.0276	6.0713	8.6119	0.1317	11.8746	↓	↑	
Hypoxanthine	POS	183.2130	137.0458	27.5073	38.4765	0.2340	6.4042	↓	↑	1,3
Pi 40:6	NEG	219.7800	909.5492	1.6204	1.2890	0.7166	1.1886	↓	↑	
Pi 36:4	NEG	222.8540	857.5182	4.5947	3.9278	1.3533	0.8006	↑	↓	
1-palmitoyl-2-linoleoyl-*rac*-glycerol	POS	223.0485	337.2738	1.6821	1.3920	1.5568	0.6718	↑	↓	
Lpe 18:2	POS	223.4810	478.2928	4.2469	3.6548	1.4426	0.7136	↑	↓	
Pi 36:3	NEG	223.9225	859.5315	4.4939	2.8696	1.8428	0.8016	↑	↓	
2-linoleoyl-1-palmitoyl-*sn*-glycero-3-phosphoethanolamine	POS	225.2520	575.5036	3.1563	1.2499	1.5001	0.8529	↑	↓	
Pi 34:2	NEG	225.3160	833.5185	3.0631	2.2888	1.5527	0.7831	↑	↓	
Xanthine	NEG	252.4680	151.0262	2.3524	2.5162	0.2698	2.6878	↓	↑	1,3,4
4-(1-piperazinyl)-1h-indole	POS	289.4630	202.1188	2.0388	1.3211	1.6509	0.7493	↑	↓	
7-methyluric acid	POS	299.9960	183.0626	1.5749	2.0400	0.4712	2.5040	↓	↑	4
gamma-hydroxybutyric acid	NEG	302.6665	103.0401	1.5126	1.4223	1.3810	0.7478	↑	↓	1,5,6
Glycine	NEG	311.0380	74.0248	2.0209	2.5339	1.2535	0.7311	↑	↓	1,3,6,7,8,9,10,11,12,13,14,15,16,17,18,19,20,21,22
Guanidoacetic acid	NEG	311.0695	116.0354	2.6839	3.3287	1.2549	0.7299	↑	↓	1,8,23
L-(+)-erythrulose	NEG	328.1390	101.0244	1.6050	2.8265	0.5973	2.2434	↓	↑	
Melibiose	NEG	340.1140	221.0669	1.04579	1.9869	0.2248	7.6943	↓	↑	1,17,24
Tetrabenazine	POS	396.8930	318.1914	1.3215	1.0916	1.3943	0.6794	↑	↓	

Note: 1. Metabolic pathways, 2. Tryptophan metabolism, 3. Purine metabolism, 4. Caffeine metabolism, 5. Butanoate metabolism, 6. Carbon metabolism, 7. Primary bile acid biosynthesis, 8. Glycine, serine and threonine metabolism, 9. Lysine degradation, 10. Phosphonate and phosphinate metabolism, 11. Glutathione metabolism, 12. Glyoxylate and dicarboxylate metabolism, 13. Thiamine metabolism, 14. Porphyrin and chlorophyll metabolism, 15. Aminoacyl-tRNA biosynthesis, 16. Biosynthesis of amino acids, 17. ABC transporters, 18. Neuroactive ligand-receptor interaction, 19. Synaptic vesicle cycle, 20. Protein digestion and absorption, 21. Mineral absorption, 22. Central carbon metabolism in cancer, 23. Arginine and proline metabolism, 24. Galactose metabolism. "↑/↓" indicate significantly increased or decreased metabolites. FC indicates "fold change".
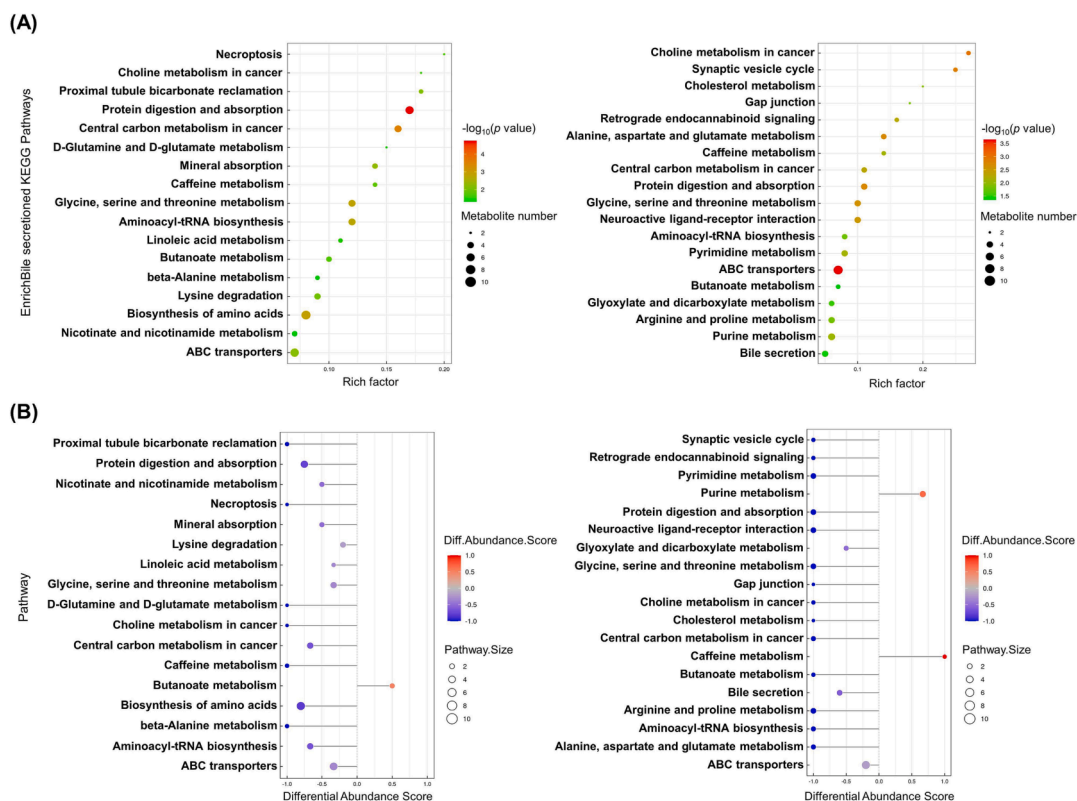
Fig. 7. KEGG pathway analysis of DEMs. (A) Bubble diagram of the KEGG enrichment pathways. Each bubble in the bubble chart represents a metabolic pathway (select the top 20 with the highest significance based on *p* value). In topology analysis, the larger the abscissa and size of the bubble, the larger the influence factor. The vertical axis and color of bubbles represent the log10 p value for the enrichment analysis. The darker the color is, the smaller the *p* value, indicating a more significant degree of enrichment. The rich factor represents the proportion of the number of DEMs in the pathway to the number of metabolites annotated in the pathway. (B) Difference abundance score map of enriched metabolic pathways. The Y-axis represents the name of the difference path, and the X-axis coordinates represent the difference abundance score (DA score). A DA score of 1 indicates an upward trend in the expression of all identified metabolites in the pathway, while −1 indicates a downward trend in the expression of all identified metabolites in the pathway. The larger the point at the end of the line segment, the more metabolites there are. The depth of the line segments and point colors is proportional to the DA score value. The darker the red color is, the more inclined the overall expression of the pathway is to increase, while the darker the blue color is, the more inclined the overall expression of the pathway is to decrease.
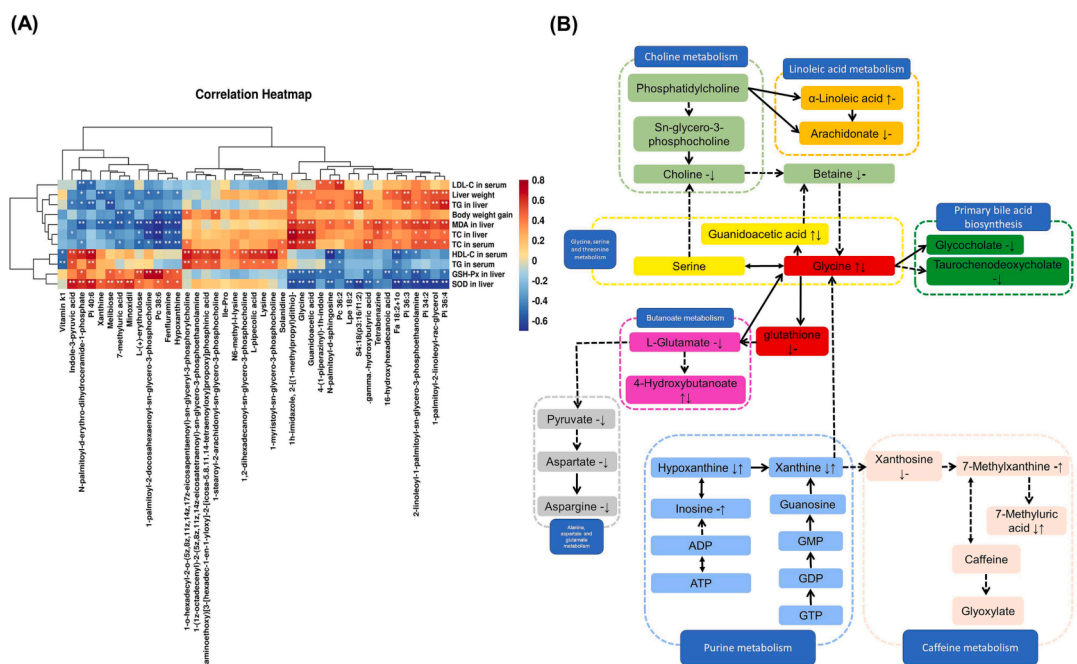

Fig. 8. (A) Spearman's correlation heatmap analysis of DEMs and metabolic syndrome-related indices. A positive correlation is in red, and a negative correlation is in blue. *p < 0.05 and **p < 0.01. (B) Metabolic network of the significantly altered metabolites associated with PVSO intervention.

acid, Fa 18:2 + 1o, Pi 36:3,2-linoleoyl-1-palmitoyl-*sn*-glycero-3-phos-phoethanolamine, Pi 34:2, and Pi 36:4 showed the opposite association ($p < 0.05$). Glycine, guanidinoacetic acid, Pi 34:2, and Pi 36:4 were also significantly positively correlated with TC levels in serum and liver ($p < 0.05$). PC 36:8, fenfluramine, and hypoxanthine were markedly negatively correlated with body weight gain, as well as TC levels in serum

and liver ($p < 0.01$). Indole-3-pyruvia acid was significantly positively correlated with SOD activity in the liver and HDL-C levels in serum ($p < 0.01$) but negatively correlated with TC and TG in the liver.
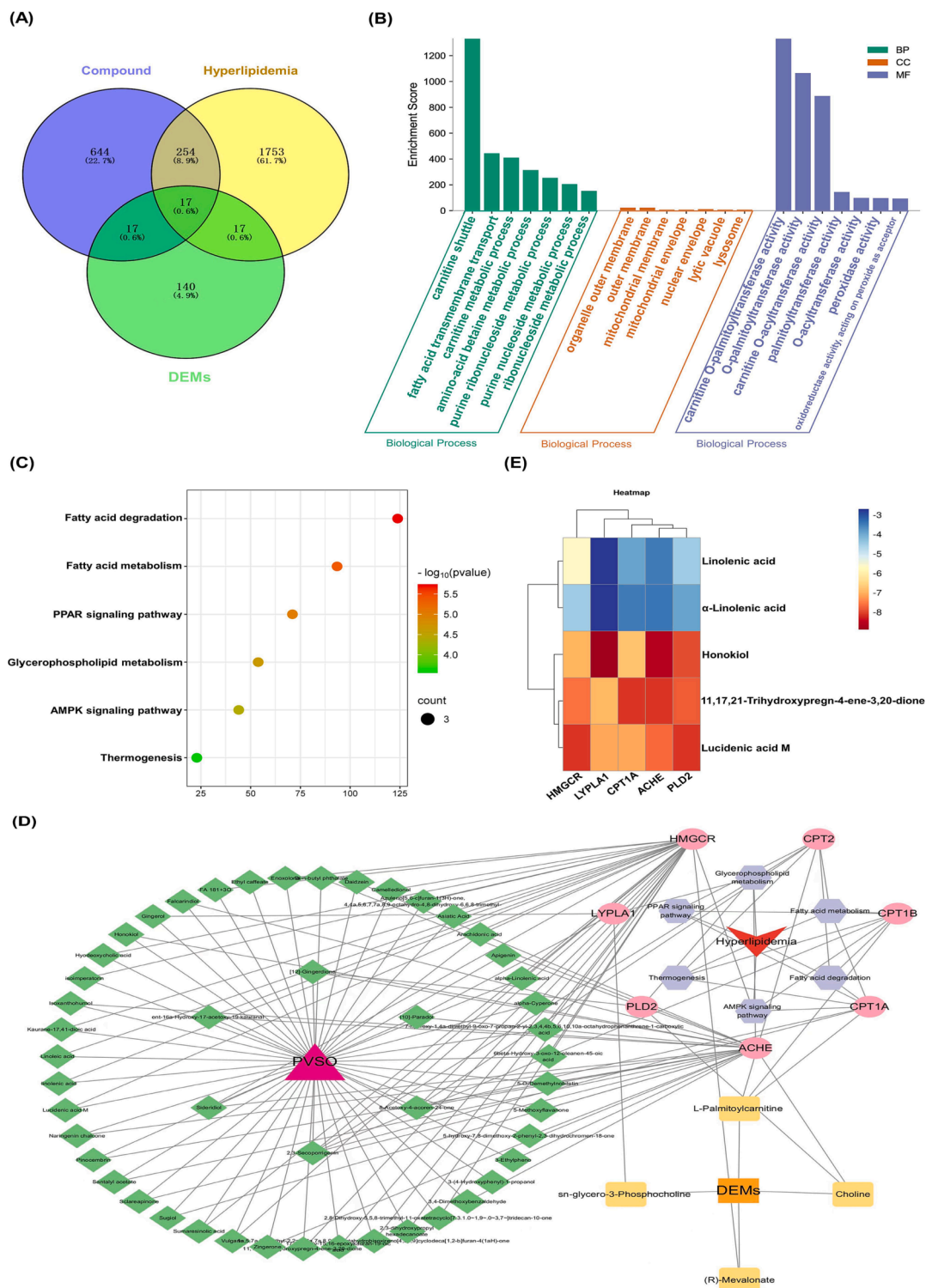

Fig. 9. Establishment of PVSO candidate ingredient-target systematic network and enrichment analyses, as well as molecular docking studies. (A) Venn diagram of component and disease related targets. (B) GO enrichment analysis. (C) KEGG pathways bubble chart. (D) "Active ingredients-Targets-KEGG pathway-Hyperlipidemia" network diagram. The red circles and blue diamonds represent the proteins and active compounds, respectively. (E) Molecular docking energy heat map of each key ingredient and each key target.

3.12. Integrative analysis of the network pharmacology and metabolomics

We constructed an interaction network based on metabolomics and network pharmacology to completely understand the mechanism of PVSO against hyperlipidemia. A total of 534 ingredients of PVSO were identified by LC-MS and GC–MS, 262 ingredients could be matched in SwissADME database, and 200 active ingredients of PVSO were obtained.

We searched "Related Targets" in the Swiss Target Prediction database to find target proteins corresponding to the 200 ingredients of PVSO. As a result, 932 targets were obtained. Prediction of hyperlipidemia disease related targets was conducted in OMIM, Gene Cards and Thermal Target Database databases, and 2040 potential targets were obtained. The DEMs between PVSO and HFD groups from serum metabolomics were input into Cytoscape's Metscape plug-in to generate a compound reaction enzyme gene network, and 191 targets were obtained. The online mapping tool was used to map the target obtained from drug prediction with the target corresponding to the disease and serum metabolomics, and the Venn map was drawn to obtain 17 intersection targets (Fig. 9A).

In the GO function enrichment analysis (Fig. 9B), a total of 21 GO entries were obtained, including 7 biological processes (BP), 7 motor functions (MF), and 7 cellular ingredients (CC). BP was significantly enriched in carnitine shuttle, fatty acid transmembrane transport, carnitine metabolic process, amino-acid betaine metabolic process, purine ribonucleoside metabolic process, etc. MF was mainly enriched in peroxidase activity, oxidoreductase activity, acting on peroxide as acceptor, etc. CC was mainly concentrated in mitochondrial membrane, lysosome, etc. The enrichment results of KEGG pathway showed that intersection targets were significantly enriched in 6 pathways ($p < 0.05$). The data showed that, PVSO mainly regulated pathways in Fatty acid degradation, Glycerophospholipid metabolism, Fatty acid metabolism, PPAR signaling pathway, AMPK signaling pathway, and Thermogenesis, indicating that the intersection targets may intervene hyperlipidemia mainly by regulating the above pathways (Fig. 9C). The top 10 targets selected by using the CytoHubba plug-in of Cytoscape 3.8.2 in the degree ranking were MPO, Crnitine palmitoyltransferase 1A (CPT1A), PTGS2, PTGS1, MGAM, ADA, XDH, CPT1B, ACHE, and CPT2. Moreover, 67 active ingredients and 31 DEMs were selected corresponding to 17 core targets. The intersection targets, active ingredients, target DEMs, and KEGG pathway were imported into Cytoscape 3.8.2 software to build a "Active ingredients-Targets-KEGG pathway-Hyperlipidemia" network (Fig. 9D). The key ingredients linolenic acid (LA), α-linolenic acid (ALA), 11,17,21-trihydroxypregn-4-ene-3,20-dione, honokiol, lucidenic acid M were selected as the core ingredients based on the degree value and relative contents, and key targets ACHE, CPT1A, 3-Hydroxy-3-methylglutaryl coenzyme A reductase (HMGCR), LYPLA1, PLD2 were obtained at the same time. Then, molecular docking analysis was conducted between these 5 key ingredients and 5 key targets.

3.13. Docking results

Based on the PPI network, the key targets (ACHE, CPT1A, HMGCR, LYPLA1, PLD2) and key ingredients (LA, ALA, 11,17,21-trihydroxypregn-4-ene-3,20-dione, honokiol, lucidenic acid M) were selected for molecular docking. The lower the binding energy between the target protein and small molecule, the more stable the binding, and the greater the possibility of action. A lower affinity represents a more stable interaction, and an affinity lower than −4.25 kcal/mol represents a threshold for interaction. In the present study, small molecules could enter the active center of target proteins, and the average binding energy was −6.164 kcal/mol. Among them, the binding energies of 11,17,21-Trihydroxypregn-4-ene-3,20-dione, honokiol, and lucidic acid M with the five potential core targets were all less than −4.25 kcal/mol. In addition, the binding energies of linolenic acid and α-linolenic acid with HMGCR were also less than −4.25 kcal/mol. This indicates that these

five active compounds may bind to five potential core targets (Fig. 9E). Through systematic analysis of PPI and molecular docking results, we found that honokiol was a candidate key ingredient of PVSO in the treatment of hyperlipidemia, and targets of LYPLA1, ACHE, as well as PLD2 ranked in the top three. Therefore, they might have a more direct relationship with honokiol. In order to further understand the binding mode of compound and protein, PyMOL software was used to visualize the compound protein interaction (each target selects the compound with the lowest binding energy).

As seen in Fig. 10 and Table 6, Honokiol bonded with the amino acid residues MET-180 and ASP-172 of LYPLA1 through hydrogen bonding. Lucidenic acid M formed five hydrogens bonded with residues LEU-509, LEU-512, TYR-514, TYR-533 and ARG-515 of HMGCR, while eight hydrogen bonds combined with amino acid residues ARG-777, LEU-438, and VAL-405. 11,17,21-trihydroxypregn-4-ene-3,20-dione formed four hydrogen bonds either with the residues GLN-413, TYR-238, PRO-235, and SER-240 of ACHE, or with the residues ARG-364, GLN-369, and VAL-370 of CPT1A, respectively. LA or ALA combined with amino acid residue ARG-178 or SER-612 of HMGCR through only one hydrogen bond.

4. Discussion

PVSO is a natural oil derived from the mature seeds of *Prunella vulgaris* L., which contains bioactive components such as unsaturated fatty acid, phenols, terpenoids, flavonoids, and squalene. However, there are no reports about the antioxidant and hypolipidemic activities of PVSO. Hence, we investigated the lipid-lowering efficacy and potential mechanisms of PVSOs through *in vivo* and *in vitro* experiments in the current study.

Dietary lipids are digested in the lumen before entering intestinal epithelial cells, where pancreatic lipase hydrolyzes triacylglycerol into 2-monoacylglycerol (2-MAG) and fatty acids, and cholesterol esterase can hydrolyze cholesterol esters into cholesterol and free fatty acids in the intestinal lumen for uptake by enterocytes (Chamnansilpa et al., 2020). In the present study, we examined the inhibitory effect of PVSO on porcine pancreatic lipase and cholesterol esterase, and the results showed that PVSO significantly inhibited the activity of porcine pancreatic lipase with an IC_{50} value of 1.68 mg/mL and cholesterol esterase with an IC_{50} value of 3.964 mg/mL. Studies have shown that polyphenols have a good inhibitory effect on pancreatic lipase, cholesterol esterase, and other digestive enzymes (Chamnansilpa et al., 2020; He et al., 2023; Jeon et al., 2014). Chen et al. (2018) proved that caffeic acid, rutin, hesperidin, ursolic acid from 80 % ethanol extract of *Prunella vulgaris* L. were with potential antagonistic effects on pancreatic lipase. PVSO mainly contains bioactive components such as unsaturated fatty acids, polyphenols, terpenoids, flavonoids, and squalene. We speculate that the inhibitory activity of PVSO against porcine pancreatic lipase and cholesterol esterase may be associated with the synergistic effect of these components.

Additionally, free cholesterol must be dissolved into micelles in the intestinal lumen for absorption. The absorption of cholesterol is highly regulated and influenced by specific compounds in the food supply. Dietary ingredients can reduce cholesterol absorption through one or more mechanisms, and mainly through the combination of bile acids and the destruction of micelles. Therefore, interfering with the formation of mixed micelles in the intestine may prevent hyperlipidemia. Some components, such as polyphenols and saponin, are known inhibitors of cholesterol absorption in the intestine (Su et al., 2016b). In our study, the addition of PVSO to cholesterol micellar solution resulted in a dose-dependent decrease in cholesterol micellar solubility. The interaction between PVSO and cholesterol may lead to an increase in particle size, inducing coprecipitation of PVSO and cholesterol in micellar solutions, thereby reducing the solubility of cholesterol and exerting a lipid-lowering effect.

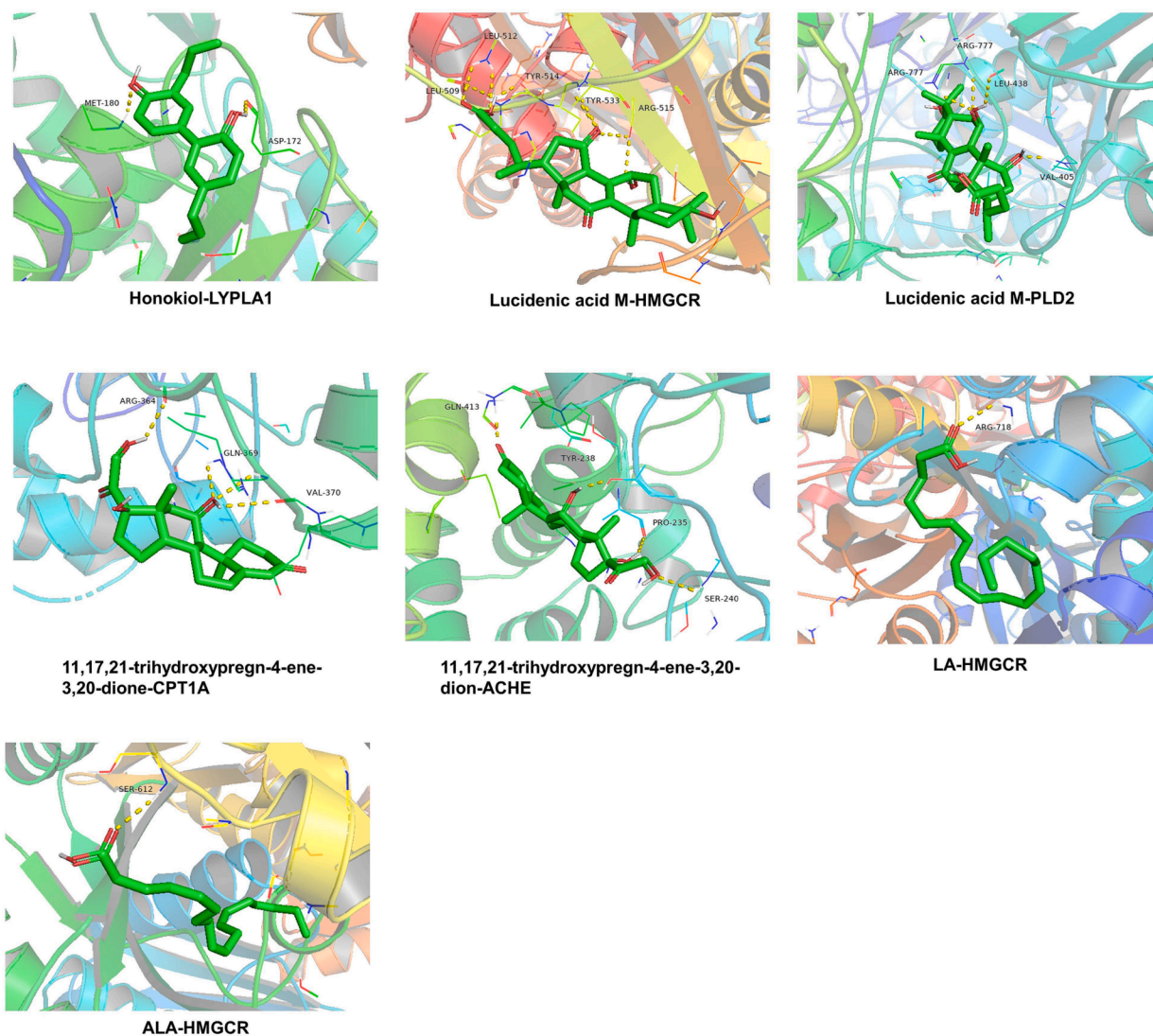Moreover, we established a HFD-induced hyperlipidemia mouse

Fig. 10. The 3D interaction diagrams of key ingredients (LA, ALA, 11,17,21-trihydroxypregn-4-ene-3,20-dione, honokiol, lucidenic acid M) and key targets (ACHE, CPT1A, HMGCR, LYPLA1, PLD2).

model and studied the effect of PVSO on hyperlipidemia through pharmacological and metabolomic analyses. Our results indicate that PVSO can significantly suppress body weight gain and inhibit increases in liver weight induced by HFD. PVSO can also reduce lipid accumulation and oxidative stress in liver tissue induced by HFD. The lipid levels in the serum and liver of mice also basically returned to equilibrium under PVSO intervention. In summary, the above results confirm the beneficial role of PVSO in improving hyperlipidemia. HFD-induced oxidative stress can induce obesity-related metabolic disorders, such as hyperlipidemia (Zhang et al., 2022a). Therefore, reducing oxidative stress may be an effective measure to prevent hyperlipidemia. In recent years, identifying lipid-lowering drugs with antioxidant potential from plants has attracted research interest, as they are normally considered to be less toxic than synthetic agents. In the present study, GSH-Px and SOD activities and relative gene expression in the livers of mice decreased significantly in the HFD group compared with the CON group, and the MDA level was significantly increased ($p < 0.05$). PVSO could inhibit lipid peroxidation and improve the activity of antioxidant enzymes, indicating that the ability to alleviate HFD-induced hyperlipidemia may be associated with its antioxidant properties and activation of the antioxidant enzyme system.

Then, by using serum metabolomics analysis, 29 metabolites were identified as the potential biomarkers related to hyperlipidemia and affected by PVSO. PVSO intervention mainly affected choline metabolism, glycine, serine and threonine metabolism pathways, and the cholesterol metabolism pathway, thereby being effective in preventing oxidative stress and lipid metabolism disorders in HFD-induced hyperlipidemia (Fig. 8B). The metabolic network of DEMs associated with PVSO intervention showed that glycine seemed to occupy a central position in the metabolic profile changes (Fig. 8B). Glycine is involved in many biological functions, as it is necessary for the synthesis of GSH, primary bile salts, heme porphyrin, creatine, and purine (Alves et al., 2019). As a cofactor of glutathione peroxidases (GPXs), GSH is involved in neutralizing H_2O_2 and lipid hydroperoxides. Researchers have found that pine leaf polysaccharides reduce the level of glycine in the serum of hyperlipidemic rats, which may protect hepatocytes from oxidative stress by promoting the synthesis of GSH from glycine (Yang et al., 2021). In this experiment, the glycine level in the HFD group increased, and the pharmacodynamic results also showed serious oxidative stress damage in the HFD group. Similarly, previous studies reported that the serum of HFD-fed individuals had high levels of glycine and low levels of GSH, which is consistent with our results (Yang et al., 2021; Jo et al., 2021; Li et al., 2022b). After PVSO intervention, the glycine level in the serum and oxidative stress damage were significantly improved.

Glycerophospholipids, including phosphatidylcholine (PC), phosphatidylethanolamine (PE) and phosphatidylserine (PS), are the most

Table 6
Dock binding free energies ($^{\Delta}$Gb) and bonds of compounds and proteins.

Protein	PDB ID	Structure	Docking compound	$^{\Delta}$Gb(kcal/mol)	Bonds formed between functional groups of compound and protein residues		
					Functional groups	Protein residues	bond
HMGCR	1DQ9		LA	−5.7	C = O	ARG-178	H-bond
			ALA	−4.5	C = O	SER-612	H-bond
			Lucidenic acid M	−8.1	−OH	LEU-509	H-bond
					C = O and −OH	LEU-512	H-bond
					−OH	TYR-514	H-bond
					−OH	TYR-533	H-bond
					−OH	ARG-515	H-bond
ACHE	5HQ3		11,17,21-trihydroxypregn-4-ene-3,20-dione	−8.1	C = O	GLN-413	H-bond
					−OH	TYR-238	H-bond
					−OH	PRO-235	H-bond
					−OH	SER-240	H-bond
CPT1A	2LE3		11,17,21-trihydroxypregn-4-ene-3,20-dione	−8.1	−OH	ARG-364	H-bond
					−OH	GLN-369	H-bond
					−OH	VAL-370	H-bond
LYPLA1	6QGN		Honokiol	−8.9	−OH	MET-180	H-bond
					−OH	ASP-172	H-bond
PLD2	7SVP		Lucidenic acid M	−8.1	−OH	ARG-777	H-bond
					−OH	LEU-438	H-bond
					−OH	VAL-405	H-bond

abundant phospholipids in mammalian cell membranes and play an important role in cell signal transduction and the lipid metabolism network (Chen et al., 2021). The disorder of glycerol phospholipid metabolism is directly related to the occurrence and development of hyperlipidemia (Ma et al., 2018). Choline is a precursor to acetylcholine, betaine, and the phospholipid backbone glycerophosphocholine (Horita et al., 2021). It has been reported that the content of phospholipid metabolites increases and phospholipid homeostasis changes in atherosclerosis model mice (Wang et al., 2023). In this experiment, the contents of betaine and PC 38:6 in the HFD group were significantly lower than those in the CON group ($p < 0.05$), while the contents of glycerophosphate choline and choline were increased ($p > 0.05$), which is consistent with many previous reports (Cai et al., 2022). However, PVSO significantly decreased the lipid metabolites of glycerophosphate metabolism, such as choline, PC 36:2, PC 38:4, and glycerophosphate choline ($p < 0.05$). Increasing evidence suggests that an increase in plasma PC levels is positively associated with fat accumulation (Kim et al., 2011). The significantly decreased PCs after PVSO intervention suggested that PVSO improved high-fat diet-induced phospholipid metabolism disorder by suppressing PC degradation and protecting the membrane (Cai et al., 2022). In addition, PE (34:2), PE (34:6), and LysoPE (18:2) were significantly enhanced in the HFD group compared to the CON group. Blood lysoPC and/or lysoPE increases were associated with atherosclerosis, oxidative stress, hyperlipidemia, and diabetes (Kim et al., 2020). Our results indicated that PVSO treatment could significantly decrease the relative content of lysoPC (16:0) ($p < 0.05$), thereby improving oxidative stress and lipid metabolism disorders induced by a high-fat diet.

Purine and pyrimidine metabolism is also related to oxidative stress and lipid metabolism (Le et al., 2013; Zhu et al., 2022b). Uric acid, xanthine, and hypoxanthine are oxidation byproducts of purine metabolism. Miao et al. (2017) found that the levels of xanthine and hypoxanthine in hyperlipidemic rats were significantly lower than those in the control group, and the concentrations of 3-methyluracil were significantly higher. The changes in xanthine and cytidine showed that DNA metabolism was abnormal, and their levels could change under certain acute and chronic pathological conditions. In the present study, the contents of xanthine, hypoxanthine, and uric acid in the PVSO group were higher than those in the HFD group ($p < 0.05$), while the contents of cytidine and uracil were lower ($p < 0.05$). Notably, uric acid is an

effective antioxidant (Tian et al., 2022). Increased serum uric acid levels could protect against oxidative stress that results in numerous human diseases and disorders (Tian et al., 2022). In addition, the content of inosine in the PVSO group was significantly increased. Inosine was found to be a purine nucleoside with extensive anti-inflammatory effects (Mao et al., 2022). Some studies have shown that inosine has lipid-lowering, antiplatelet, anti-inflammatory and vasodilative effects in hypercholesterolemia animal models, and its mechanism may be through inhibiting the MAPK/NF-κB signaling pathway (Lima et al., 2020).

In this study, we combined network pharmacology and metabolomics to select the active ingredients of PVSO and related targets linked with hyperlipidemia. Molecular docking was carried out to validate predicted targets. ACHE, CPT1A, HMGCR, LYPLA1, and PLD2 were the key targets of PVSO against hyperlipidemia. Reportedly, an increase in AChE activity occurred when lipid metabolism was abnormal and oxidative stress was enhanced (Yamchuen et al., 2014). Chia seed oil or kiwifruit seed oil administration may modulate lipid metabolism and oxidative stress via up-regulated the expression of liver PPARα and CPT1A in HFD-induced hyperlipidemia or obese mice (Han et al., 2020; Qu et al., 2019). Tetracarpidium conophorum (African walnut) Seed Oil, Grape Seed Oil, Peony Seed Oil all showed a hypolipidemic effect by inhibiting HMGCR activities (Oriakhi et al., 2020; Ebrahimi-Mameghani et al., 2020; Su et al., 2016a). In our study, LA, ALA, 11,17,21-trihydroxypregn-4-ene-3,20-dione, honokiol, and lucidenic acid M in PVSO, especially honokiol, exerted good docking abilities with the above key target proteins. The results of molecular docking were consistent with the results of network pharmacology. Numerous studies have confirmed that honokiol has a wide range of biological activities, including anti-inflammatory, antioxidant properties, and regulating lipid metabolism (Liu et al., 2020). In addition to anti-cancer, anti-inflammatory, anti-oxidant, anti-viral, anti-obesity, anti-diabetic, neuroprotective, and immunomodulatory properties, it also has been proved that lucidenic acids could improve hyperlipidemia (Zheng et al., 2023). Another study has shown that lucidenic acid E can inhibit HMG-CoA reductase (Chen et al., 2017). Therefore, it is speculated that these active ingredients may be important material basis of PVSO to treat hyperlipidemia.

Additionally, according to the findings of the KEGG pathway analysis, PVSO primarily inhibits the occurrence and development of hyperlipidemia via the Fatty acid degradation and metabolism pathway,

PPAR signaling pathway, Glycerophospholipid metabolism pathway, AMPK signaling pathway, and Thermogenesis pathway, which are closely linked to the lipid metabolism as reported. Thus the regulation of these pathway may be beneficial for the treatment of hyperlipidemia and merits further exploration.

5. Conclusion

P. vulgaris is an edible herb originally distributed in Europe and Asia that is now widespread in Africa, America and Australia and has been used as herbal tea, food, dietary supplement or medicinal plant for several centuries. PVSO is a natural oil derived from the mature seeds of *P. vulgaris* that contains bioactive components such as unsaturated fatty acid (with a ratio of linolenic acid to linoleic acid of 3:1), phenols, terpenoids, flavonoids, and squalene. The extraction rate of PVSO by supercritical CO_2 extraction reached 16.63 %. Our findings demonstrated that PVSO plays a role in improving hyperlipidemia, which may be due to inhibiting the activities of pancreatic lipase and cholesterol esterase, as well as inhibiting the solubility of cholesterol micelles, thus leading to the inhibition of cholesterol absorption. On the other hand, our study provides evidence that PVSO supplementation can alleviate lipid metabolism disorders and liver oxidative stress response in HFD-fed mice. These functions are related to the regulation of choline metabolism, glycine, serine and threonine metabolism pathways, cholesterol metabolism pathways and so on. ACHE, CPT1A, HMGCR, LYPLA1, and PLD2 were the key targets of PVSO against hyperlipidemia. LA, ALA, 11,17,21-trihydroxypregn-4-ene-3,20-dione, honokiol, and lucidenic acid M in PVSO, exerted good docking abilities with the above key target proteins. This is the first report on the biological activity of PVSO. Hence, all these findings led us to hypothesize that PVSO could serve as a potential natural functional ingredient to reduce the risk of hyperlipidemia, which highlights the real health-promoting potential of PVSO.

Authorship contribution statement

Z.Z. and J.X. designed and funded the project; X.Q., T.Y., Z.L., M.Z., C.L., S.T., S.Z., and T.X. performed the experiment; Z.Z. and X.Q. analyzed and interpreted the data; Z.Z., X.Q., Z.L., and S.T. wrote the original draft; Z.Z. and P.W. revised the manuscript. All authors have read and agreed to the published version of the manuscript.

Ethics statement

The animal study was reviewed and approved by the Institutional Animal Care and Use Committee, Hunan University of Chinese Medicine.

Declaration of Competing Interest

The authors declare that they have no known competing financial interests or personal relationships that could have appeared to influence the work reported in this paper.

Appendix A. Supplementary data

Supplementary data to this article can be found online at https://doi.org/10.1016/j.arabjc.2023.105486.

References

Ahmed, N.F., Sadek, K.M., Soliman, M.K., Khalil, R.H., Khafaga, A.F., Ajarem, J.S., Allam, A.A., 2020. Moringa oleifera leaf extract repairs the oxidative misbalance following sub-chronic exposure to sodium fluoride in Nile tilapia Oreochromis niloticus. Animals 10 (4), 626–644.

Alves, A., Bassot, A., Bulteau, A.L., Pirola, L., Morio, B., 2019. Glycine metabolism and its alterations in obesity and metabolic diseases. Nutrients 11 (6), 1356.

Bai, Y., Xia, B., Xie, W., Zhou, Y., Xie, J., Li, H., Li, C., 2016. Phytochemistry and pharmacological activities of the genus *Prunella*. Food Chem. 204, 483–496.

Björnsson, E.S., 2017. Hepatotoxicity of statins and other lipid-lowering agents. Liver Int. 37 (2), 173–178.

Cai, H., Wen, Z., Xu, X., Wang, J., Li, X., Meng, K., Yang, P., 2022. Serum metabolomics analysis for biomarkers of Lactobacillus plantarum FRT4 in high-fat diet-induced obese mice. Foods 11 (2), 184.

Chamnansilpa, N., Aksornchu, P., Adisakwattana, S., Thilavech, T., Mäkynen, K., Dahlan, W., Ngamukote, S., 2020. Anthocyanin-rich fraction from Thai berries interferes with the key steps of lipid digestion and cholesterol absorption. Heliyon 6 (11), e05408.

Chen, T.G., Li, L.Y., Wei, Y.R., Zhang, L.W., 2018. Screening, Identification and Activity Evaluation of Pancreatic Lipase Inhibition in *Prunella Vulgaris*. Zhongguo Zhong Yao Za Zhi 43 (23), 4665–4671.

Chen, B., Tian, J., Zhang, J., Wang, K., Liu, L., Yang, B., Liu, H., 2017. Triterpenes and meroterpenes from Ganoderma lucidum with inhibitory activity against HMGs reductase, aldose reductase and α-glucosidase. Fitoterapia 120, 6–16.

Chen, S., Wu, Q., Zhu, L., Zong, G., Li, H., Zheng, H., Sun, L., 2021. Plasma glycerophospholipid profile, erythrocyte n–3 PUFAs, and metabolic syndrome incidence: a prospective study in Chinese men and women. Am. J. Clin. Nutr. 114 (1), 143–153.

Danthine, S., Aman, P., Jansen, O., Ducrey, A., Richel, A., Lognay, G., Frédérich, M., 2022. *Prunella vulgaris* L. seeds: a promising source of lipids, proteins, and original phenolic compounds presenting high antioxidant and anti-inflammatory activity. Biotechnol. Agron. Soc. 26 (1).

Deng, J., Li, L., Yan, J., Lin, L.M., Li, Y.M., Lin, Y., Xia, B.H., 2022. Essential oil from *Prunella vulgaris* L. as a valuable source of bioactive constituents: In vitro anti-bacterial, anti-viral, immunoregulatory, anti-inflammatory, and chemical profiles. S. Afr. J. Bot. 151, 614–627.

Du, X., Bai, M., Huang, Y., Jiang, Z., Chen, F., Ni, H., Li, Q., 2018. Inhibitory effect of astaxanthin on pancreatic lipase with inhibition kinetics integrating molecular docking simulation. J. Funct. Foods 48, 551–557.

Ebrahimi-Mameghani, M., Irandoost, P., Pourmoradian, S., 2020. The Effects of Grape Seed Oil on the Cardiovascular Risk Factors in Overweight and Obese Women: A Double-Blind Randomized Clinical Trial. Curr. Top. Nutraceut. r. 18 (3), 221–227.

Gan, X.J., Liu, S.P., Liu, Z.F., Hu, X.L., Tian, J., Xue, J.X., 2013. Fluorescence quenching method for the determination of carbazochrome sodium sulfonate with aromatic amino acids. Luminescence 28 (3), 265–269.

Gosis, B.S., Wada, S., Thorsheim, C., Li, K., Jung, S., Rhoades, J.H., Arany, Z., 2022. Inhibition of nonalcoholic fatty liver disease in mice by selective inhibition of mTORC1. Science 376 (6590), eabf8271.

Han, K., Li, X.Y., Zhang, Y.Q., He, Y.L., Hu, R., Lu, X.L., Hui, J., 2020. Chia seed oil prevents high fat diet induced hyperlipidemia and oxidative stress in mice. Eur. J. Lipid Sci. Tech. 122 (4), 1900443.

He, X., Chen, L., Pu, Y., Wang, H., Cao, J., Jiang, W., 2023. Fruit and vegetable polyphenols as natural bioactive inhibitors of pancreatic lipase and cholesterol esterase: Inhibition mechanisms, polyphenol influences, application challenges. Food Biosci. 103054.

Horita, D.A., Hwang, S., Stegall, J.M., Friday, W.B., Kirchner, D.R., Zeisel, S.H., 2021. Two methods for assessment of choline status in a randomized crossover study with varying dietary choline intake in people: Isotope dilution MS of plasma and in vivo single-voxel magnetic resonance spectroscopy of liver. Am. J. Clin. Nutr. 113 (6), 1670–1678.

Huang, X., Zhu, J., Wang, L., Jing, H., Ma, C., Kou, X., Wang, H., 2020. Inhibitory mechanisms and interaction of tangeretin, 5-demethyltangeretin, nobiletin, and 5-demethylnobiletin from citrus peels on pancreatic lipase: Kinetics, spectroscopies, and molecular dynamics simulation. Int. J. Biol. Macromol. 164, 1927–1938.

Jeon, S.Y., Imm, J.Y., 2014. Lipase inhibition and cholesterol-lowering activities of laccase-catalyzed catechin polymers. Food Sci. Biotechnol. 23, 1703–1707.

Jesch, E.D., Carr, T.P., 2017. Food ingredients that inhibit cholesterol absorption. Prev. Nutr. Food Sci. 22 (2), 67–80.

Jo, J.K., Seo, S.H., Park, S.E., Kim, H.W., Kim, E.J., Kim, J.S., Son, H.S., 2021. Gut microbiome and metabolome profiles associated with high-fat diet in mice. Metabolites 11 (8), 482.

Khafaga, A.F., 2017. Exogenous phosphatidylcholine supplementation retrieve aluminum-induced toxicity in male albino rats. Environ. Sci. Pollut. Res. 24 (18), 15589–15598.

Kim, H.J., Kim, J.H., Noh, S., Hur, H.J., Sung, M.J., Hwang, J.T., Yoon, S.H., 2011. Metabolomic analysis of livers and serum from high-fat diet induced obese mice. J. Proteome Res. 10 (2), 722–731.

Kim, M., Yoo, H.J., Ko, J., Lee, J.H., 2020. Metabolically unhealthy overweight individuals have high lysophosphatide levels, phospholipase activity, and oxidative stress. Clin. Nutr. 39 (4), 1137–1145.

Kind, T., Wohlgemuth, G., Lee, D.Y., Lu, Y., Palazoglu, M., Shahbaz, S., Fiehn, O., 2009. FiehnLib: mass spectral and retention index libraries for metabolomics based on quadrupole and time-of-flight gas chromatography/mass spectrometry. Anal. Chem. 81 (24), 10038–10048.

Le, T.T., Ziemba, A., Urasaki, Y., Hayes, E., Brotman, S., Pizzorno, G., 2013. Disruption of uridine homeostasis links liver pyrimidine metabolism to lipid accumulation. J. Lipid Res. 54 (4), 1044–1057.

Lee, J.H., Lee, Y.Y., Lee, J., Jang, Y.J., Jang, H.W., 2021. Chemical composition, antioxidant, and anti-inflammatory activity of essential oil from omija (Schisandra chinensis (Turcz.) Baill.) produced by supercritical fluid extraction using CO2. Foods 10 (7), 1619.

Li, L., Deng, J., Lin, L.M., Li, Y.M., Lin, Y., Xia, B.H., Liao, D.F., 2022a. Metabolomics and pharmacodynamic analysis reveal the therapeutic role of *Prunella vulgaris* oil on intrauterine adhesion rats. J. Pharmaceut. Biomed. 209, 114532.

Li, L., Tian, Y., Feng, Y., Zhang, S., Jiang, Y., Zhang, Y., Wang, C., 2022b. Improvement in mung bean peptide on high-fat diet-induced insulin resistance mice using untargeted serum metabolomics. Front. Nutr. 9, 893270.

Lima, G.F., de Oliveira Lopes, R., Mendes, A.B.A., Brazão, S.C., Autran, L.J., Motta, N.A. V., Brito, F.C., 2020. Inosine, an endogenous purine nucleoside, avoids early stages of atherosclerosis development associated to eNOS activation and p38 MAPK/NF-kB inhibition in rats. Eur. J. Pharmacol. 882, 173289.

Liu, Y., Cheng, P., Wu, A.H., 2020. Honokiol inhibits carotid artery atherosclerotic plaque formation by suppressing inflammation and oxidative stress. Aging 12 (9), 8016–8028.

Liu, W., Jiang, K., Wang, J., Mei, T., Zhao, M., Huang, D., 2021. Upregulation of GNPNAT1 predicts poor prognosis and correlates with immune infiltration in lung adenocarcinoma. Front. Mol. Biosci. 8, 605754.

Long, X., Hu, X., Xiang, H., Chen, S., Li, L., Qi, B., Yang, X., 2022. Structural characterization and hypolipidemic activity of Gracilaria lemaneiformis polysaccharide and its degradation products. Food Chem. x. 14, 100314.

Ma, N., Liu, X.W., Kong, X.J., Li, S.H., Jiao, Z.H., Qin, Z., Li, J.Y., 2018. Aspirin eugenol ester regulates cecal contents metabolomic profile and microbiota in an animal model of hyperlipidemia. BMC Vet. Res. 14 (1), 405.

Mao, B., Guo, W., Tang, X., Zhang, Q., Yang, B., Zhao, J., Zhang, H., 2022. Inosine pretreatment attenuates LPS-induced lung injury through regulating the TLR4/MyD88/NF-κB signaling pathway *in vivo*. Nutrients 14 (14), 2830.

Martinez-Gonzalez, A.I., Alvarez-Parrilla, E., Díaz-Sánchez, Á.G., de la Rosa, L.A., Núñez-Gastélum, J.A., Vazquez-Flores, A.A., Gonzalez-Aguilar, G.A., 2017. In vitro inhibition of pancreatic lipase by polyphenols: A kinetic, fluorescence spectroscopy and molecular docking study. Food Technol. Biotech. 55 (4), 519–530.

Miao, H., Zhang, L., Chen, D.Q., Chen, H., Zhao, Y.Y., Ma, S.C., 2017. Urinary biomarker and treatment mechanism of *Rhizoma Alismatis* on hyperlipidemia. Biomed. Chromatogr. 31 (4), e3829.

Ogawa, K., Hirose, S., Nagaoka, S., Yanase, E., 2016. Interaction between tea polyphenols and bile acid inhibits micellar cholesterol solubility. J. Agric. Food Chem. 64, 204–209.

Onwe, P., Folawiyo, M., Anyigor-Ogah, C.S., Umahi, G., Okorocha, A.E., Afoke, A., 2015. Hyperlipidemia: etiology and possible control. IOSR J. Dent. Med. Sci. 14 (10), 93–100.

Oriakhi, K., Uadia, P., 2020. Hypolipidemic Activity of Tetracarpidium conophorum (African walnut) Seed Oil and Its Mechanism of Action. Planta Med. 7 (04), e170–e178.

Pan, J., Wang, H., Chen, Y., 2022. *Prunella vulgaris* L.–a review of its ethnopharmacology, phytochemistry, quality control and pharmacological effects. Front. Pharmacol. 13, 903171.

Qu, L., Liu, Q., Zhang, Q., Liu, D., Zhang, C., Fan, D., Yang, H., 2019. Kiwifruit seed oil ameliorates inflammation and hepatic fat metabolism in high-fat diet-induced obese mice. J. Funct. Foods 52, 715–723.

Qu, Z., Zhang, J., Yang, H., Gao, J., Chen, H., Liu, C., Gao, W., 2017. *Prunella vulgaris* L., an Edible and Medicinal Plant, Attenuates Scopolamine-Induced Memory Impairment in Rats. J. Agric. Food Chem. 65, 291–300.

Su, J., Ma, C., Liu, C., Gao, C., Nie, R., Wang, H., 2016a. Hypolipidemic activity of peony seed oil rich in α-linolenic, is mediated through inhibition of lipogenesis and upregulation of fatty acid β-oxidation. J. Food Sci. 81 (4), H1001–H1009.

Su, J., Wang, H., Ma, C., Liu, C., Gao, C., Nie, R., Tanver Rahman, M.R., 2016b. Hypocholesterolaemic mechanism of bitter melon aqueous extracts via inhibition of pancreatic cholesterol esterase and reduction of cholesterol micellar solubility. Int. J. Food Sci. Nutr. 67 (1), 20–28.

Sun, L., Chen, W., Meng, Y., Yang, X., Yuan, L., Guo, Y., 2016. Interactions between polyphenols in thinned young apples and porcine pancreatic α-amylase: Inhibition, detailed kinetics and fluorescence quenching. Food Chem. 208, 51–60.

Zhu, W.W., Tang, C.H., 2022a. Mild preheating improves cholesterol-lowering benefits of soy protein via enhancing hydrophobicity of its gastrointestinal digests: An *in vitro* study. Food Hydrocolloid. 124, 107282.

Zhu, Y., Zhang, Y., Li, Y., Guo, C., Fan, Z., Li, Y., Wang, J., 2022b. Integrative proteomics and metabolomics approach to elucidate metabolic dysfunction induced by silica nanoparticles in hepatocytes. J. Hazard. Mater. 434, 128820.

Ta, N., A., L., E., E., Qi, R., Mu, X., Feng, L., Ba, G., ... & Fu, M., 2023. Metabolomics analysis reveals amelioration effects of yellowhorn tea extract on hyperlipidemia, inflammation, and oxidative stress in high-fat diet-fed mice. Front. Nutr. 10, 1087256.

Tian, R., Yang, C., Chai, S.M., Guo, H., Seim, I., Yang, G., 2022. Evolutionary impacts of purine metabolism genes on mammalian oxidative stress adaptation. Zool Res. 43 (2), 241–254.

Vermeer, M.A., Mulder, T.P., Molhuizen, H.O., 2008. Theaflavins from black tea, especially theaflavin-3-gallate, reduce the incorporation of cholesterol into mixed micelles. J. Agric. Food Chem. 56 (24), 12031–12036.

Wang, S., Sun, Z., Dong, S., Liu, Y., Liu, Y., 2014. Molecular interactions between (-)-epigallocatechin gallate analogs and pancreatic lipase. PLoS One 9 (11), e111143.

Wang, Y., Sun, X., Qiu, J., Zhou, A., Xu, P., Liu, Y., Wu, H., 2023. A UHPLC-Q-TOF-MS-based serum and urine metabolomics approach reveals the mechanism of Gualou-Xiebai herb pair intervention against atherosclerosis process in ApoE$^{-/-}$ mice. J. Chromatogr. b. 1215, 123567.

Wierzbicki, A.S., Hardman, T.C., Viljoen, A., 2012. New lipid-lowering drugs: an update. Int. J. Clin. Pract. 66 (3), 270–280.

Yamchuen, P., Aimjongjun, S., Limpeanchob, N., 2014. Oxidized low density lipoprotein increases acetylcholinesterase activity correlating with reactive oxygen species production. Neurochem. Int. 78, 1–6.

Yang, X.L., Li, L., Zhang, T.F., Deng, J., Lin, X.L., Li, Y.M., ... & Lin, L.M., 2021. GC-MS-Based Serum Metabolomic Investigations on the Ameliorative Effects of Polysaccharide from Turpiniae folium in Hyperlipidemia Rats. Oxid. Med. Cell. Longev. 2021.

Zhang, Y., Hao, J., Liu, Z., Li, Z., Teng, L., Wang, D., 2022a. Inonotus hispidus Protects against Hyperlipidemia by Inhibiting Oxidative Stress and Inflammation through Nrf2/NF-κB Signaling in High Fat Diet Fed Mice. Nutrients 14 (17), 3477.

Zhang, H.L., Wu, Q.X., Wei, X., Qin, X.M., 2020. Pancreatic lipase and cholesterol esterase inhibitory effect of Camellia nitidissima Chi flower extracts *in vitro* and *in vivo*. Food Biosci. 37 (3), 100682–100688.

Zhang, Z., Xie, Z., Lv, S., Shi, Y., Zhai, C., Li, X., Gao, X., 2022b. Integrated metabolomics and network pharmacology study on the mechanism of Kangfuxiaoyan suppository for treating chronic pelvic inflammatory disease. Front. Pharmacol. 13, 812587.

Zhang, J., Zhang, W., Mamadouba, B., Xia, W., 2012. A comparative study on hypolipidemic activities of high and low molecular weight chitosan in rats. Int. J. Biol. Macromol. 51 (4), 504–508.

Zhao, S.Y., Liu, Z.L., Shu, Y.S., Wang, M.L., He, D., Song, Z.Q., Liu, Y.Y., 2017. Chemotaxonomic Classification Applied to the Identification of Two Closely-Related Citrus TCMs Using UPLC-Q-TOF-MS-Based Metabolomics. Molecules 22 (10), 1721.

Zheng, C., Rangsinth, P., Shiu, P.H., Wang, W., Li, R., Li, J., Leung, G.P., 2023. A Review on the Sources, Structures, and Pharmacological Activities of Lucidenic Acids. Molecules 28 (4), 1756.

Zhou, X., Liu, L., Lan, X., Cohen, D., Zhang, Y., Ravindran, A.V., Xie, P., 2019. Polyunsaturated fatty acids metabolism, purine metabolism and inosine as potential independent diagnostic biomarkers for major depressive disorder in children and adolescents. Mol. Psychiatr. 24, 1478–1488.